THESIS

POLY (ADP-RIBOSE) POLYMERASE 1 (PARP1) AND ITS DNA-BINDING CHARACTERISTICS

Submitted by

Michael A. Kramer

Department of Biochemistry and Molecular Biology

In partial fulfillment of the requirements

For the Degree of Master of Science

Colorado State University

Fort Collins, Colorado

Spring 2011

Master's Committee:

Advisor: Karolin Luger

Robert Woody
Susan Bailey

ABSTRACT

POLY (ADP-RIBOSE) POLYMERASE 1 (PARP1) AND ITS DNA-BINDING CHARACTERISTICS

The poly(ADP-ribose) polymerase (PARP) family is evolutionarily diverse, containing 18 different protein members. Roles played by PARP1 in the cell appear to be significant in establishing cellular complexity, as a correlation exists between higher eukaryotes and prevalence of PARP family members. Each member of the PARP family contains a conserved catalytic domain, which upon activation cleaves molecules of NAD^+ to form polymers of ADP-ribose, with the release of nicotinamide. Poly(ADP-ribosyl)ation reactions carried out by PARP family members have been found to function in regulation of cellular systems including DNA-damage repair, transcription, mitotic spindle formation, telomere maintenance and cell-death signaling.

The most well established member of the PARP family is poly(ADP-ribose) polymerase 1 or PARP1. PARP1 has been found to associate with an assortment of DNA structures within the cell. Despite being able to complex with any DNA present in the cell, PARP1 displays a propensity to interact with sites of

DNA-damage. As such, PARP1 has been found to play a major role in initiation of DNA-damage repair. Through its catalytic activity PARP1 recruits additional DNA-damage repair machinery and promotes exposure of the site of damage through chromatin relaxation. Due to its ability to regulate chromatin structure, PARP1 has also been frequently connected with transcription regulation. Variable regulation of transcription by PARP1 has been observed. Catalytically inactive PARP1 can function in a similar fashion as the protein H1 to condense chromatin. Alternatively, active PARP1 functions to relax chromatin surrounding promoter regions and recruit transcription machinery.

PARP1 activity appears to be primarily regulated through its association with DNA. Little is known regarding PARP1-DNA-binding affinity. Here I present a high-throughput in-solution FRET-based assay that I utilize to better characterize PARP1's interaction with sites of DNA-damage. In addition, the PARP1-nucleosome complex was analyzed utilizing the same FRET-based assay. Discrepancies found between PARP1 binding affinities to various DNA-damage and mononucleosome constructs provide insight into a potential variable mode of interaction exhibited by PARP1.

ACKNOWLEDGEMENTS

I would like to convey my extreme gratitude to Dr. Karolin Luger. I have been a member of the Luger lab for over three years. My time in the Luger lab has provided me with knowledge and experience that will serve me in both professional and personal endeavors. In addition, I would like to thank all past and present members of the Luger lab for their continuous support and teachings. I would like to express a special thanks to Mary Robinson, Keely Sudhoff, Wayne Lilyestrom and Nick Clark for their tolerance of my inquisitiveness and individuality.

Additionally, I would like to send much thanks to my committee members, Dr. Woody and Dr. Bailey. Dr. Woody has acted as my student advisor throughout my undergraduate and graduate career. I would like to thank him for his support and wisdom throughout the years. I would also like to display appreciation for Dr. Bailey and our many conversations that provided additional perspectives that assisted me in my project time and time again.

DEDICATION

I would like to dedicate the work presented here to my mother, father, brother and Aunt Carol, who have provided constant inspiration and motivation. Any success I have obtained, or will procure in the future, is due to their unwavering support and guidance.

TABLE OF CONTENTS

BIOLOGICAL RELEVANCE

Poly(ADP-Ribose) polymerase 1 (PARP1) is the second most abundant protein in eukaryotes. PARP1 plays a role in many cellular processes including DNA-damage repair, gene regulation, chromatin modification and dynamics, mitotic spindle formation, and cell-death signaling [1, 2]. In addition, PARP1 has been a target in the field of medicine due to its links to cardiovascular disease, ischemic stroke, septic shock, diabetes, inflammation control, and cancer treatment [3, 4].

PARP1 contains an N-terminal DNA-binding domain followed by a BRCT domain and a C-terminal catalytic domain [1]. PARP1's catalytic domain catalyzes the production of nicotinamide and polymers of ADP-ribose (PAR) from NAD^+ and ATP substrates [1]. PARP1's catalytic activity is linked to the majority of its functions within the cell. It has been shown that PARP1 catalytic activation is dependent upon recognition and binding of DNA [2, 5]. To date, no substantial binding characterization of the PARP1-DNA complex exists.

I have developed a high-throughput FRET-based binding assay in order to quantitate the interaction of PARP1 with DNA. I used DNA constructs that mimic typical sites of damage within the cell, as well as constructs deviating from the traditional double helical structure. Additionally, the interaction of PARP1 with the nucleosome was assessed. Our data suggest that PARP1 uses different binding modes to interact with the different DNA constructs and with nucleosomes. This provides insight into the multifaceted binding capabilities exhibited by PARP1. Furthermore, the observed discrepancies are analogous with the diverse roles of PARP1 within the cell. This correlation may help elucidate a more global understanding of the PARP1 mechanism of action.

BACKGROUND

Poly (ADP-Ribose) Polymerase 1

The large PARP family has 18 protein members expressed from different genes. Each member of the PARP family contains a conserved PARP catalytic domain [1]. PARP1 and PARP2 exist as the only known members with an immediate role in DNA-damage signaling and repair [1]. The best-characterized PARP family member is PARP1.

PARP1 is a 1014-residue protein containing a flexible hinge region that acts to connect the DNA-binding region and auto-modification domain of PARP1 to the conserved PARP family catalytic domain. PARP1's DNA-binding domain consists of two homologous Zn finger motifs and a Zn ribbon domain [1, 6]. Adjacent to the Zn finger motifs is a BRCT domain common to proteins associated with DNA-damage repair. Connected to the PARP1 DNA-binding domain by a flexible hinge region exists a poorly classified WGR domain, followed by the PARP catalytic domain (Figure 1A) [1].

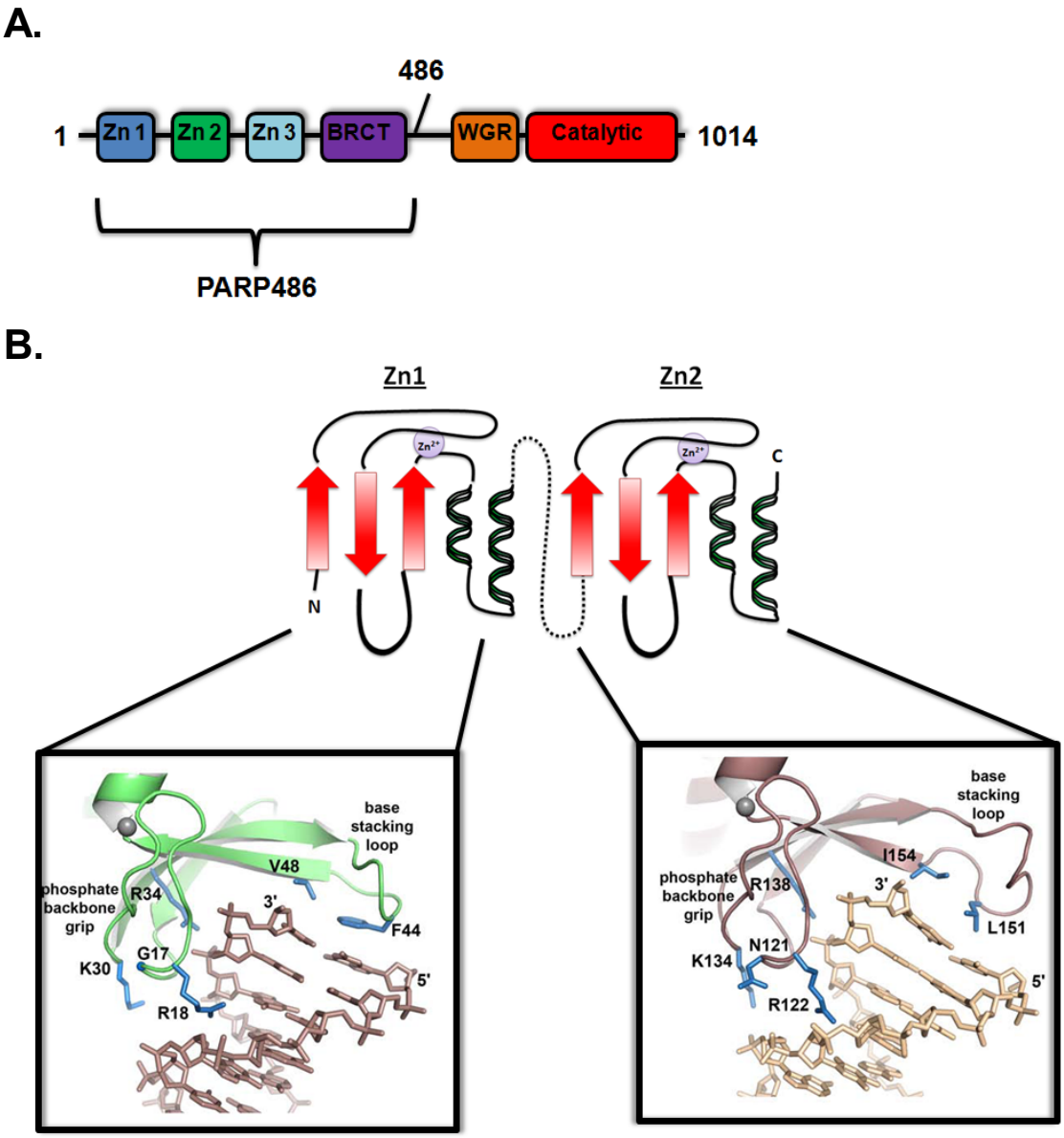

Figure 1- PARP1 contains two Zn fingers comprised within its DNA binding domain that are connected via a flexible hinge region to the PARP catalytic domain. **(A)** PARP1 is composed of three zinc-containing domains (two Zn fingers and a Zn ribbon fold) and a BRCT domain connected by a flexible hinge region to its WGR domain and a catalytic domain conserved throughout the PARP family. **(B)** A recent crystal structure displays interactions made by the two Zn finger motifs of PARP1 with blunt-ended DNA through a hydrophobic base stacking loop and a charged phosphate backbone grip region. Crystal structures of Zn fingers in complex with DNA adapted from Langelier *et al.,* J Biol Chem, 2011. 286(12): p. 10690-10701.

The catalytic domain present at PARP1's C-terminus converts molecules of NAD^+ to polymers of ADP-ribose in reactions targeting assorted cellular proteins, in addition to auto-modification of its own BRCT domain [1, 2, 7]. Poly(ADP-ribos)ylation (PARylation) of protein targets, such as the DNA-damage repair protein XRCC1 and histones H2A and H1, act to initiate and regulate various cellular pathways. In addition, PARP1 has been shown to function via heterodimerization with proteins through its BRCT domain [1, 7].

Catalytic activity of PARP1 is activated upon binding to DNA containing blunt ends, internal nicks and overhang regions [8]. Recent crystallography and NMR data indicate that PARP1 interaction with blunt-ended DNA is mediated through hydrophobic loops contained on each Zn finger [9]. Structural data also indicates that electrostatic contacts made by charged residues of the Zn fingers with the DNA phosphodiester backbone act in stabilizing the PARP1-DNA complex (Figure 1B) [9]. It has been proposed that PARP1 activation is dependent on a conformational change across the hinge region induced by the binding of the zinc-finger containing domains to sites of DNA-damage [8]. PARP1 activation facilitates catalysis of poly (ADP-ribosyl)ation reactions targeted to multiple proteins, including DNA-repair proteins, core histones, linker histone H1 and itself [10-12].

Cellular response to DNA-damage

Although prevalent in many cellular processes, PARP1 functions primarily in DNA-damage repair initiation and signaling cell-death pathways in the presence of widespread DNA-damage. Genetic information manifested as DNA within each cell is pivotal to cellular function and replication. As such, the cell spares no expense in its response to and repair of DNA-damage. DNA integrity is susceptible to frequent attack by a plethora of agents that are generated by routine cellular metabolism and environmental factors. DNA malformations are induced by improper incorporation of dNTPs during DNA replication, DNA deamination, depurination and alkylation, as well as by exposure to reactive oxygen species (ROS). Environmental damage is also prevalent as the cell is subjected to external factors such as ionizing radiation (IR) and UV light [7, 13-15].

Single-strand breaks (SSBs) and double-strand breaks (DSBs) are encountered regularly in the cell. Numerous cellular pathways are devoted to the repair of such DNA-damage. Repair pathways dealing with SSBs include mismatch repair (MMR), which corrects improperly incorporated base pairs, and base-exclusion repair (BER), which targets chemically modified nucleotides [7]. Nucleotide-excision repair (NER), which identifies and removes regions exhibiting extensive

damage, acts through DSB intermediates. Lesions in the form of DSBs are repaired through non-homologous end joining (NHEJ) and homologous recombination (HR) [7].

The complexities of DNA-damage repair are further compounded by the range of proteins involved in each pathway. Tight regulation of repair pathways is essential to ensure cellular competence. In order to prevent DNA-damage proliferation, a close relationship is held between DNA-damage repair and cell-death [1, 13, 15]. This relationship ensures removal of any cell species exhibiting exhaustive DNA-damage or faulty repair mechanisms. Members of the phosphoinositide-3-kinase-related protein kinase (PIKK) family (ATM, ATR and DNA-PK) and the PARP family are largely responsible for recognition of sites of DNA-damage and signaling of either repair pathways or cellular apoptosis and senescence through intermediates like p53 [1, 13, 15].

PARP1-dependent DNA-damage repair pathways

Base-Exclusion Repair Pathway

Although linked to multiple SSB repair pathways, PARP1 is most widely associated with base-exclusion repair (BER), an important pathway in the correction DNA base damage. BER targets and repairs damaged genomic DNA

through a SSB intermediate. Two types of BER exist within the cell, short-patch and long-patch BER [7]. In short-patch repair a DNA glycosylase recognizes the site of damage and converts it to an apurinic/apyrimidinic (AP) site. Apurinic/apyrimidinic endonuclease 1 (APE1) then recognizes the newly formed AP site and cleaves the phosphodiester bond, yielding a nick in the DNA with a 5' deoxyribose phosphate and a 3' hydroxyl group. The 5'-deoxyribose phosphate is then removed and the correct Watson-Crick base pair is inserted by DNA polymerase β (Pol β). Upon proper insertion of the correct nucleotide, DNA Ligase III seals the nick [7].

Long-patch repair occurs when the 5'-deoxyribose phosphate has undergone oxidation or reduction. If an oxidized or reduced 5'-deoxyribose phosphate is present, long-patch repair acts to displace the 5'-deoxyribose phosphate via a 5'-flap structure. This pathway involves additional factors, including flap endonuclease 1 (FEN1) and proliferating cell nuclear antigen (PCNA) [7].

PARP1 and SSB repair

PARP1's role in SSB repair has been the subject of widespread investigation. In the most widely accepted model for PARP1's involvement in SSB repair, PARP1 recognizes nicked regions of DNA, presumably following APE1 cleavage of AP sites in BER [1, 2]. Upon binding, PARP1 is activated, catalyzing a series of PARylation reactions using NAD^+ as its substrate. Active PARP1 functions to

increase accessibility to the site of damage through relaxation of the surrounding chromatin. PARP1 achieves chromatin decondensation through PARylation reactions targeting nearby H2A and H1 histones, promoting relaxation of chromatin surrounding the site of damage (Figure 2B). In addition, PARP1 targets itself in an auto-PARylation reaction, creating a large PAR network stemming from its own BRCT domain. Through this mechanism PARP1 recruits additional BER factors including XRCC1, DNA ligase III, and Pol β to the site of damage [1, 2, 16]. Recruitment occurs through PAR modification of the factor, interaction with the produced branched PAR moiety or via protein-protein interactions with the PARP1 BRCT domain (Figure 2B) [1, 2]. Once a threshold of auto-PARylation is met, PARP1 will dissociate from the DNA allowing the recruited factors to complete the repair process through nucleotide insertion and DNA-strand ligation. Chromatin compaction then occurs as a PAR-hydrolyzing enzyme, poly(ADP-ribose) glycohydrolase (PARG), cleaves the remaining PAR network surrounding the site of damage (Figure 2C) [1].

Additional models of PARP1 SSB-repair association are different in the mode and chronology of PARP1 recruitment to sites of damage. One such model depicts PARP1 as a negative regulator of long-patch repair. Sukhavnova et al. demonstrated a correlation between long-patch repair inhibition and PARP1 localization to DNA, while observing no such inhibition of short-patch repair by PARP1. They also noted that auto-PARylation of PARP1 significantly reduced inhibition of long-patch repair [17].

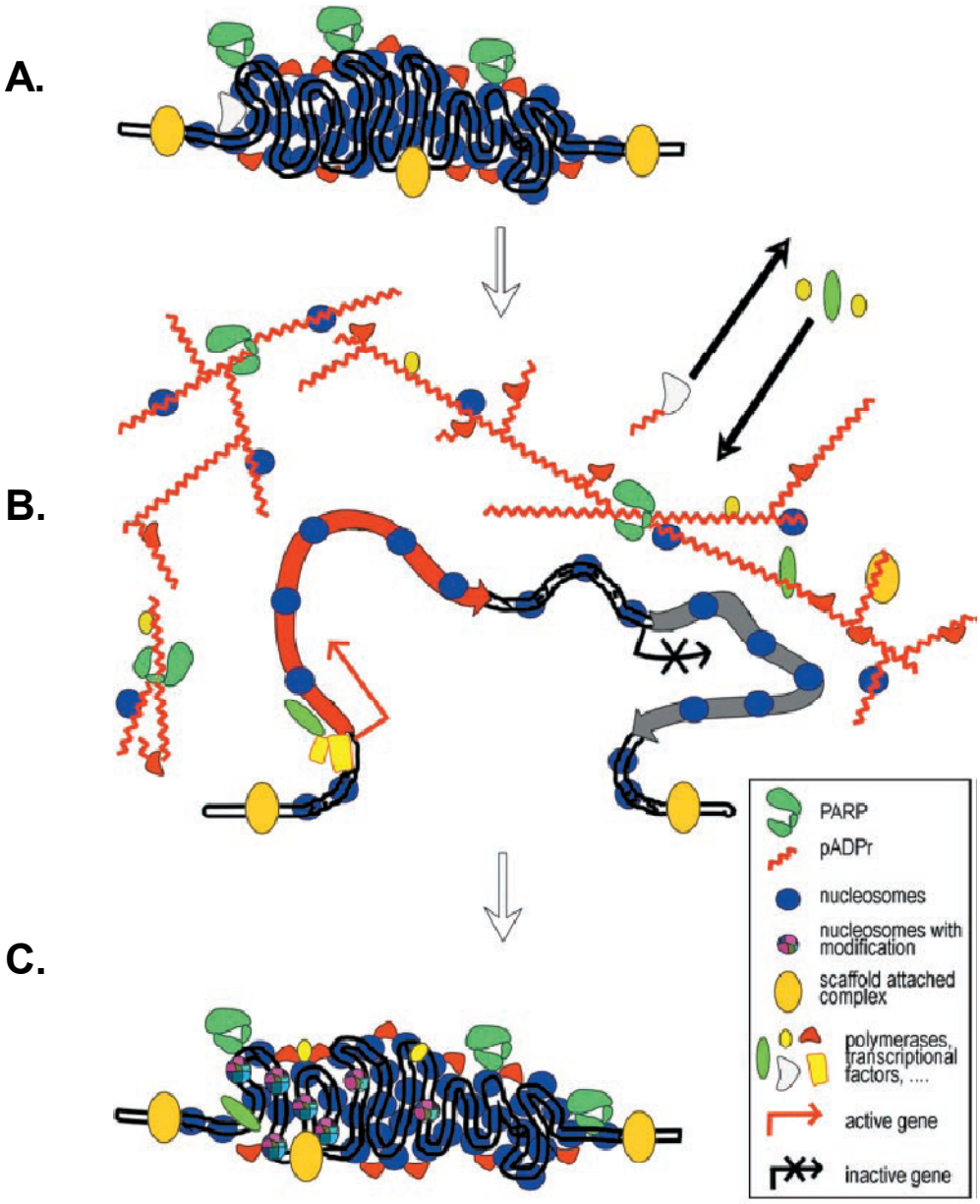

Figure 2 - A model of PARP1-mediated chromatin loosening at sites of DNA damage. (A) PARP1 **(green)** interacts with condensed chromatin when catalytically inactive. **(B)** Upon recognition of DNA damage the PARP1 enzymatic domain catalyzes poly(ADP-ribosyl)ation **(red)** of core histones **(blue)** proximal to the site of damage, generating a relaxed chromatin structure. PARylation reactions catalyzed by PARP1 recruit DNA-damage repair factors to the now exposed site of damage. **(C)** Upon completion of DNA-damage repair, auto-inactivation of PARP1 through self-modification and the degradation of PAR molecules by PARG return the chromatin to its condensed state **(C)**. Adapted from Tulin *et al.,* Science. 2003. 299(5606): p. 560-562.

Recently, the Helleday group observed a lack of SSB accumulation following exposure to an alkylating agent in cells depleted of PARP1 using siRNA. The introduction of alkylating agent induced DNA-damage sites similar to what is targeted in BER. Failure to generate an increase in SSB's in PARP1 depleted cells led the Helleday group to conclude that PARP1 plays no direct role in BER. They propose an alternative function in which PARP1 acts in a repair enhancement fashion [18]. The Helleday group suggests that past literature is likely skewed by the use of PARP1 inhibitors in control groups. PARP1 inhibitors obstruct any catalytic activity of PARP1, but in the process also trap PARP1 in complex with DNA. This trapping of PARP1 to the site of damage may impair additional components of BER from recognizing the site, leading to a lack of DNA-repair resolution [18].

Non-Homologous End Joining

Non-homologous end joining (NHEJ) is a major DNA-damage repair pathway responsible for the repair of DSB's in cellular DNA. NHEJ maintains activity throughout the cell cycle and is important for V(D)J recombination and for repair of endogenously and exogenously induced DSBs [19]. NHEJ corrects DSBs through ligation of the two cleaved DNA ends. This process is initiated by Ku70/Ku80 alignment of severed DNA ends. Ku70/Ku80 then recruits DNA-PK and activates its kinase function. DNA-PK in association with Artemis and other

processing proteins then prepare the DNA ends for ligation through the addition of a 5'-phosphate group. At this point XRCC4 in complex with DNA ligase IV, join the broken strands together [20].

PARP1 competes with Ku70/Ku80 for the site of damage, potentially signaling an alternative-NHEJ mechanism through recruitment of the MRN complex [21]. This alternative-NHEJ mechanism is prevalent when NHEJ factors are absent or malfunctioning [22].

Homologous Recombination

Homologous recombination (HR) is the second of the two PARP1-associated DSB repair pathways. HR conservatively and accurately repairs DSBs though utilization of the damaged sequence's sister chromatid [20]. As such, HR functions in S phase and G_2 phase of the cell cycle [20, 23]. HR functions by first processing portions of each DNA end, producing 3'-ssDNA overhangs. Rad51 will then match homologous DNA from the sister chromatid to the repair site. Strand exchange will then occur via Holliday junction formation [20].

PARP1 maintains a dual relationship with HR. DNA-replication forks pause when encountering SSBs. The SSB is then cleaved to a DSB and repaired by HR before the replication fork can restart [1, 2, 24]. PARP1's role in initiation of SSB-

repair pathways leads to the repair of DNA-damage prior to their recognition by replication forks and subsequent propagation to DSBs. Thus, PARP1 indirectly inhibits the HR pathway through initiation of SSB repair.

Paradoxically, PARP1 also has been linked to HR initiation at stalled replication forks. Repair of DSBs present at replication forks is dependent on PARP1 in complex with MRN and ATM [25]. The MRN/PARP1/ATM complex is required for the DNA strand resection involved in HR. Once the DSB is repaired the replication machinery will reinitiate and continue beyond the newly repaired DNA [25].

Chromatin dynamics and gene regulation

Approximately two meters of DNA exist within an 8 μm cell nucleus. This remarkable feat is accomplished through the packaging of genomic DNA into protein-DNA complexes known as chromatin. In its most basic form, chromatin exists in a ‘beads on a string’ formation in which the fundamental units of chromatin, nucleosomes, are separated by a given amount of linker DNA. This beads on a string structure becomes further compacted into a 30-nm chromatin fiber, which forms its final tertiary structure through additional intermolecular contacts with itself.

The nucleosome is composed of 147 bp of DNA wrapped 1.65 times around a protein histone octamer [26]. The histone octamer is composed of a H3-H4 histone tetramer and two H2B-H2A dimers [27]. An additional histone, H1, is also associated with the nucleosome. H1 promotes compaction through interaction with linker DNA and the nucleosome dyad [28]. Each core histone is composed of an α-helical folded region and a highly disordered N-terminal 'tail' region. The ordered fold region of each histone interacts with DNA, while the disordered N-terminal tails are responsible for interactions between adjacent nucleosomes [26]. In addition, modifications of the histone tails play important roles in regulation of the dynamic chromatin structure [29].

Regulation of chromatin dynamics is essential for proper gene expression and DNA-damage repair. In order for the genetic material to be readily available, chromatin structure must be highly dynamic, alternating between a condensed and relaxed state. Highly condensed chromatin, termed heterochromatin, is inaccessible to transcription and DNA-repair machinery. For transcription and DNA-damage repair machinery to gain access to genomic DNA, chromatin must convert to its more loosely packed state, euchromatin. Chromatin dynamics are regulated through histone-tail modification, chromatin remodeling complexes, histone chaperones, and incorporation of histone variants.

PARP1 and gene expression

PARP1 interacts with nucleosomes in a manner similar to H1. Although the exact mechanism of each is a subject of speculation, both serve to regulate function in determining nucleosome spacing and chromatin dynamics [30, 31]. H1 and PARP1 compete for binding to nucleosomes, indicating that both display similar affinities for regions in close proximity along the nucleosome [32]. Interestingly, a trend is observed at transcribed promoters, in which a decrease in H1 presence is observed concomitant with an increase in PARP1 localization [32].

PARP1 displays contrasting roles in chromatin dynamics. Inactive PARP1 associates with chromatin in the nucleus when experiments are performed under steady-state conditions [31, 33]. In cells in which PARP1 has been knocked out, a significant change in overall chromatin compaction is observed. Intriguingly, despite its global effect on chromatin compaction, PARP1 plays a dual role in transcription leading to activation of certain genes while repressing others [34, 35].

When catalytically inactive, PARP1 functions to inhibit gene expression through compaction of chromatin found at gene promoter regions [30]. Inactive PARP1 also expels the chromatin-compaction protein H1 at various PARP1-stimulated genes. Following expulsion of H1 and association of PARP1 to chromatin surrounding the gene promoter, gene expression is stimulated as PARP1

becomes activated. PARylation of histone targets by PARP1 allows transcription machinery to gain access to the promoter due to decondensation of surrounding chromatin. It is possible that inactive PARP1 expels H1 and associates with genes in a poised state, maintaining compaction of promoter chromatin until signaled to activate and promote expression. It is important to note that at genes in which the presence of PARP1 is tied to repression, no pattern of H1 and PARP1 colocalization are observed [36]. Additional effects of PARP1 on transcription regulation have been tied to PARP1 interactions with transcription machinery [16, 32, 35, 38, 44].

In addition to direct histone PARylation, PARP1 catalytic activity has been tied to histone acetylation and H4 Lys4 trimethylation (H3K4me3) [35]. The mode of PARP1 regulated gene expression remains unclear, but multiple mechanisms have been proposed. The most simplistic mechanism of transcriptional regulation is through PARP1's ability to PARylate core histones. PAR carries a large negative charge and as such is likely to promote relaxation of chromatin due to PAR-DNA charge repulsion [37]. Additionally, PARP1 may control transcription of certain genes through its recruitment of the transcriptional machinery. A correlation between PARP1 and recruitment of TBP, TFIIB and Pol II at given promoters has been observed [16, 32]. PARP1 has also been found to interact with proteins of the ERK transcription regulation pathway. Active PARP1 interacts directly with ERK2, which increases ERK2 phosphorylation of ERK1. Phosphorylated ERK2 promotes an increase of histone acetylation at the target

promoter, up-regulating gene expression [38]. Furthermore, PARP1 catalytic activity has been linked to H3K4me3. Upon PARP1 knockdown, the Kraus group observed a decrease in H3 methylation at PARP1-activated genes and an increase in methylation at PARP1-inhibited genes, with no effect on PARP1 independent genes [35]. They propose a mechanism in which PARP1 PARylates and inhibits promoter binding of KDM5B, a lysine-specific histone demethylase.

It is clearly evident that PARP1 plays a multifaceted role in chromatin dynamics, in which it exhibits positive and negative gene regulation function. Gene expression and repression by catalytically active and inactive PARP1, respectively, suggests a dual function that is dependent upon PARP1 interaction with particular genes, or chromatin as a whole. PARP1 may contribute to indiscriminate nucleosome spacing and chromatin condensation in its inactive form, while regulating target genes via its catalytic activity upon activation.

PARP1's additional roles in the cell

PARP1 promotes cell-death when extensive DNA-damage is present (Figure 3). Upon DNA-damage recognition, PARP1 signals formation of a Rad9, Rad1, Hus1 complex [13]. This complex is then activated upon Rad17 stimulation and produces a cascade of signals involving the serine/threonine-protein kinases ATM and ATR. The cascade terminates upon signaling of various cell-cycle

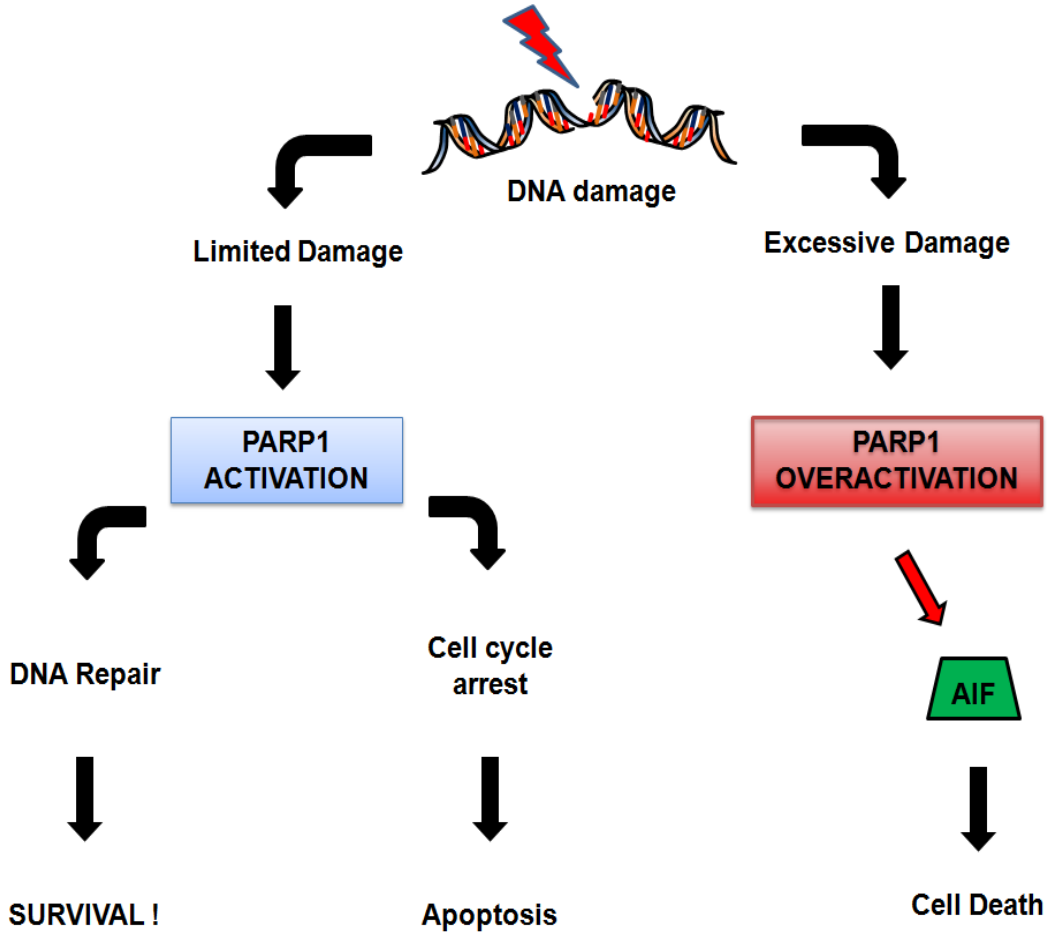

Figure 3- PARP1 activation at sites of DNA-damage signals repair mechanisms or death pathways. In replicating cells, limited DNA damage leads to PARP1 activation and signaling of repair pathways. During p53 signaling of apoptosis, caspases cleave PARP1, inhibiting signaling of repair pathways as the cell proceeds towards cell death. In cells exhibiting excessive DNA damage, overactivation of PARP1 leads to NAD^+ depletion, along with translocation of Apoptosis-Inducing Factor (AIF) to the nucleus.

check-points including histone H2AX, CHK2 and p53. Once signaled, the cell-cycle check-points induce cell-cycle arrest. Subsequent death or rejuvenation depends on the cell's ability to successfully repair the site of damage [1, 13].

PARP1 is also involved in cell-death when stimulated by excessive ROS [13, 39]. PARylation by PARP1 consumes NAD^+ and ATP as substrates. Cellular depletion of NAD^+ and ATP due to highly active PARP1 can promote cell-death by necrosis (Figure 3). In response to excess ROS, PARP1 may also trigger apoptosis through interaction with apoptosis-inducing factor (AIF) [39]. In this poorly understood mechanism, PARP1 activation can trigger the release of AIF from mitochondria. AIF will then target to the nucleus where it induces chromatin condensation and DNA fragmentation [39].

Other PARP family members play important roles in maintaining genome stability. For example, PARP family members Tankyrase 1 and Tankyrase 2 play major roles in maintaining telomere integrity [40]. Telomere maintenance is essential for cell survival, as critical shortening of telomeres leads to cell senescence and death [40]. Additionally, telomeres exist as the DNA termini of chromosomes, and are logical targets of PARP1 interaction, as PARP1 is known to interact with DNA ends. In mice engineered for PARP1 knockdown, telomere shortening is observed [41]. In addition, when uncapped telomeres are induced by the G4 ligand RHPS4, PARP1 activation and localization to the uncapped

telomeres occurs [41, 42]. It has been shown that PAR units produced by PARP1 at uncapped telomeres are associated with telomere-repeat binding factor I (TRF1). PARP1 has also been found to interact directly with TRF2 and PARylate telomere-associated protein POT1 [42, 43]. PARP1's telomere-associated functions are thought to assist in telomere repair and maintenance.

PARP1, along with five other members of the PARP family, including Tankyrase 1 and 2, are also associated with various components of the mitotic apparatus (PARP2, PARP3, VPARP, tankyrase1, and tankyase2) [44]. PARP1 has been shown to associate with mitotic centromeres, centrosomes, and mitotic spindles. Although its function is poorly understood, regulation of PARylation appears pivotal to control of mitotic functions. One proposed function of PAR molecules is in assembly and orientation of bipolar spindles [44]. It has been suggested that PARylation may act as a signaling mechanism in regulation of mitotic spindle proteins, or in the formation of a matrix that is utilized in spindle assembly [44]. Involvement of active and inactive PARP1 with additional cellular functions and pathways continues to be investigated.

Förster Resonance Energy Transfer (FRET)

In 1948 Theodore Förster refined a theory outlining dipole-dipole energy transfer that was originally proposed by Jean-Baptiste Perrin in 1927 [45-47]. Perrin's dipole-dipole energy transfer theory was presented as a possible explanation of

depolarization of fluorescence in dye solutions at high concentrations [47]. Perrin hypothesized that energy transfer between an excited molecule and a nearby molecule could occur without needing physical contact and without the emission and absorption of a photon. This energy transfer would occur through interaction of oscillating dipoles from two molecules in close proximity [47]. Over 20 years following Perrin's initial hypothesis, Förster published his first paper on Förster resonance energy transfer, or FRET, in which he expanded upon Perrin's preliminary findings to produce the first correct theoretical description of the FRET process [47]. In this paper, Förster developed a theory in which one could quantitate rate and efficiency of energy transfer between donor and acceptor molecules [46, 47].

E. R. Blout and Lubert Stryer went on to confirm Förster's theories on FRET and apply them at the molecular level as a 'spectroscopic ruler' [48, 49]. This application is possible due to Förster's theory of efficiency of energy transfer (E) as governed by the equation:

$$E = \frac{1}{1 + (r / R_o)^6}$$

where *r* is the distance between the donor and acceptor and R_o is the distance at which the efficiency of transfer is 50% [46]. Intensity of emission by the acceptor molecule can be applied to the characterization of structure and dynamics of macromolecular interactions. Additionally, FRET is highly sensitive as it is able to

monitor systems ranging from high micromolar to low nanomolar concentrations [50]. FRET is presently utilized in many experimental systems, ranging from analysis of *in vivo* protein-protein interactions to *in vitro* quantification of protein-DNA affinities [50].

Caution must be imposed when utilizing FRET in binding experiments to ensure data validity due to the nature of data collection. FRET emission spectra following donor-acceptor energy transfer also contains basal level contribution from non-FRET invoked donor and acceptor emission. Energy transfer from donor to acceptor molecules is not a 100% efficient process, leaving a degree of donor emission that contributes to the overall FRET signal. Additionally, acceptor molecules are also excited directly by wavelengths that are used to excite donor molecules. This may also generate contribution to the overall FRET spectra through acceptor emission independent of the FRET mechanism. As a result, experimental methods incorporating FRET must carefully account for any donor and acceptor contribution through signal normalization. Adequate normalization is performed through controls unique to each FRET reaction system.

When employed correctly, FRET can be a powerful tool, as I demonstrate here with its use in PARP1-DNA-binding studies. To determine PARP1 affinities to DNA, a donor fluorophore was added to the PARP1 protein and an acceptor fluorophore was added its DNA substrate. Affinities were then determined after

imaging titration reactions performed in a 384-well microplate. The sensitivity provided by FRET allowed for detailed analysis of PARP1's binding affinity to various DNA substrates. Additionally, due to the versatility of the FRET system developed, we were able to display that full-length PARP1 binds with higher affinity than a $Parp_{1-486}$ truncation construct to DNA-damage substrates and nucleosomes. Results obtained by FRET allow us to propose a mechanism in which PARP1 activity may be driven by differences in its binding affinity to the different DNA substrates.

METHODS

Cloning, expression and purification of $Parp_{1-486}$

The first 486 residues of PARP1 plus an N-terminal 6x histidine tag were cloned into a pET28a vector system (Novagen). $Parp_{1-486}$ was expressed in *E. coli* BL43 cells after cells grew to an absorbance of 0.6-0.8. Expression proceeded for 5 hr at 30º C. 6 L of cells were resuspended in 100 mL of lysis buffer (300 mM NaCl, 25 mM Tris pH 7.0) containing a single tablet of protease inhibitor cocktail (Roche). Following cell lysis via sonication, the protein was bound to a Ni-NTA fast flow column (Qiagen). Ni resin with bound protein was washed three times with 50 mL of resuspension buffer (200mM NaCl, 25 mM Tris pH 7.0, 25 mM imidazole). The protein was eluted from the Ni column using 300 mM imidazole, 200 mM NaCl, and 25 mM Tris pH 7.0. Protein was further purified using Hightrap-SP cation-exchange column (GE Healthcare), followed by S75 size-exclusion chromatography.

Fluorescent labeling of $Parp_{1-486}$

Purified full-length PARP1, $Parp_{1-486}$ and $Parp_{487-1014}$ were fluorescently labeled on their intrinsic cysteine residues. 10 mM Alexa-488 fluorophore (Invitrogen) in

DMSO was added to protein in 300mM NaCl, 25mM Tris pH 7.5 in equimolar amounts three times over three hours and allowed to mix overnight to ensure a high efficiency of labeling. Free fluorophore in-solution was separated using a Hightrap-Heparin HP cation-exchange column (GE Healthcare).

DNA oligomer preparation

Blunt-ended, nicked, gap, and overhang DNA all containing the template sequence 5'- ATC AGA TAG CAT CTG TGC GGC CGC TTA GGG -3' and with labeled sequences containing a 5'-Cy5 fluorophore were ordered from Integrated DNA Technologies (IDT). Blunt-ended DNA reverse sequence was the complement of the template sequence. Overhang sequence reverse sequence was 5'-ATC AGA CCC TAA GCG GCC GCA CAG ATG CTA-3' with the first 6bp of the reverse and template sequence remaining single stranded upon annealing. AATT-insert DNA was identical to the blunt-ended sequence with a 5'-AATT-3' nucleotide substitution of bases 14-17. Nicked and gapped DNA's were generated through deletion of a central base pair or introduction of a break in the phosphodiester backbone in the reverse sequence. Annealing was carried out through 2 min. heating at 95º C of equimolar template and reverse strand, followed by slow cooling to room temperature.

EMSA

Protein-DNA and protein-nucleosome complexes were assayed for stoichiometry and affinity analysis using 5% native acrylamide gels. Gels were run in 50 mM Tris-Borate buffer at pH 8.8. Gels were visualized without stain under UV-light prior to staining with ethidium bromide and Coomasie blue stain.

FRET assay

In-solution based FRET assays were done with Alexa488 labeled PARP1 as fluorescent donor, and with DNA or nucleosome labeled with Cy5 or Atto647 as fluorescent acceptor. DNA was labeled as stated above and nucleosomes were labeled at an incorporated E63C mutation located in the H4 histones. Each assay depicts a 23-point DNA or nucleosome titration to constant [PARP1] (5-10 fold below measured Kd); each assay was performed in duplicate. Unless otherwise stated, the reaction buffer contained 200mM NaCl, 25mM Tris pH 7.5, 0.01% CHAPS, 0.01% NP40. Reactions were performed in 384-well microplates (Greiner bio-one) treated with 2% 1,6-dichlorooctamethyl-tetrasiloxane (in 98% heptane) to reduce non-specific interactions. Reactions were imaged using Typhoon Trio™ Variable Mode Imager (GE Healthcare).

FRET was quantified following excitation of donor molecules (using a 488 nm laser) through observation of acceptor emission, using a 670/15 emission band filter. In order to account for spectral overlap by donor and acceptor molecules in FRET spectra, donor and acceptor controls were implemented. The donor control consisted of wells containing donor held at a constant concentration (equal to [donor] in FRET reaction wells) in the absence of acceptor. To account for an increase in spectral overlap of acceptor throughout the FRET titration series, normalization to acceptor signal was carried out using entire titration series of acceptor without donor. Donor and acceptor controls were imaged using laser and filter settings specific to excitation and emission of donor and acceptor fluorophores at 3mm focal length (Donor – 488 nm excitation, 520/20 nm emission band filter; Acceptor - 632 nm excitation, 670/15 nm emission band filter).

FRET calculations

Donor and acceptor spectral overlap in the FRET signal was accounted for through normalization to percent signal contribution. Percent contribution was calculated through comparison of donor or acceptor signal to FRET signal in donor only and acceptor only wells. Final plotted values were normalized using the obtained percent donor and acceptor contribution according to the following equation:

$$FRETc = FRET - [(Dc \times FRET) + (Ac \times FRET)]$$

where FRETc is final corrected FRET signal, FRET is total signal obtained using FRET excitation and emission settings, and Dc and Ac are percent contribution to overall FRET signal due to donor (D) and acceptor (A). Normalized FRET replicate values were averaged and plotted in Prism software using:

$$\text{Plotted FC} = \frac{Fc}{Fc + Dc}$$

where Fc is normalized FRET counts and Dc is donor counts. Kd's were calculated by curve fits to the normalized FRET data using the Prism software.

RESULTS

Abstract

The most studied of the evolutionarily conserved PARP family is poly (ADP-ribose) polymerase 1 or PARP1. PARP1 plays important roles in DNA-damage repair, transcription regulation, mitotic spindle formation, telomere maintenance and cell-death signaling. PARP1 is a 1014-residue protein comprised of a DNA-binding region, BRCT domain, WGR domain and the catalytic domain conserved throughout the PARP family. When active, PARP1 catalyzes the conversion of NAD^+ to polymers of ADP-ribose. Active PARP1 can add ADP-ribose units to many cellular proteins, but its major target is itself. Auto poly(ADP-ribosyl)ation exhibited by PARP1 functions as a pathway signaling mechanism, as well as a form of self-regulation.

PARP1 plays a major role in DNA-damage signaling and as expected has been found to associate with sites of DNA-damage such as double-strand breaks (DSB) and single-strand breaks (SSB). Analysis of PARP1's mode of interaction with sites of DNA-damage is limited in the literature. In order to better understand the PARP1-DNA interaction we have developed a highly sensitive FRET-based

assay to procure PARP1's binding affinity to various DNA constructs. We observe a binding preference for DNA constructs displaying similar structural characteristics to SSB's.

The PARP1-nucleosome interaction was also assessed utilizing the same FRET-based assay. A higher binding affinity to mononucleosomes by full-length PARP1 than a truncation mutant containing only the DNA-binding domain of PARP1 was observed. These results suggest that while the DNA-binding domain of PARP1 is necessary and sufficient for PARP1 binding, domains located at the C-terminus of PARP1 significantly contribute to the interaction with mononucleosomes.

Introduction

Proteins interact with DNA in the cell to mediate processes such as transcription and DNA-damage repair. Protein-DNA interactions are regulated in order to ensure proper cellular function. Regulation is primarily performed through catalysts, inhibitors, variable chromatin structure, protein translocation and the manner of DNA interaction. Protein-DNA interactions occur in a DNA-specific or non-specific manner. Classification and strength of interaction are driven by how structural motifs of the protein make contact with DNA. Protein interactions will occur with base pairs via the major and minor groove, or with the negatively charged phosphodiester backbone. In addition to DNA-sequence specificity,

proteins have been shown to display increased affinity to specific DNA structure. For example, histones, HMG protein and TATA binding protein (TBP) preferentially interact with DNA regions displaying higher flexibility [51-53].

DNA-binding domains interact electrostatically and/or form hydrogen bonds with groups in the phosphodiester backbone or the nucleotides. DNA-binding proteins typically contain a helix-turn-helix motif, leucine-zipper coiled-coil, β-ribbon, helix-loop-helix motif, or Zn-containing domain [54]. Often DNA-associated proteins contain multiple DNA-binding domains to enhance DNA-binding capability.

PARP1 associates with DNA to carry out the majority of its cellular functions. PARP1 contains a DNA-binding domain N-terminally located to its BRCT, WGR and catalytic domains. PARP1's DNA-binding domain is composed of three Zn-containing motifs: two Zn-fingers and a Zn ribbon fold consisting of three β-sheets and two terminal α-helices. Each Zn-containing motif is interconnected by loop regions variable within the PARP family, which have been proposed to play a role in DNA-substrate specificity [1, 6]. Despite the incorporation of well-characterized Zn motifs much is still to be determined regarding the means in which PARP1 recognizes and binds to DNA.

PARP1 is a highly basic protein composed of a combined 193 Arg and Lys residues, with a pI of 8.99. Additionally, a role in DNA-binding has been proposed for the associated WGR and catalytic (WGR-Cat) domains located at the C-terminus of PARP1 [55]. Although the WGR-Cat region of PARP1 contains no known DNA-binding motifs, it is possible its overall positive charge mediates an interaction with the negatively charged DNA phosphodiester backbone. It is likely that the basic WGR-Cat regions are not involved directly in DNA recognition and binding, but rather act to stabilize the primary interaction between DNA and the Zn-finger motifs.

None of the Zn-containing motifs in the PARP1 DNA-binding domain have been found to exhibit DNA sequence specificity. Alternatively, PARP1 Zn-fingers have been shown to associate with archetypical DNA-damage structures, such as DNA nicks, overhangs and gaps [1, 2]. In addition, PARP1 has been found to recognize DNA with distinct secondary structure such as hairpin loops and DNA cruciforms [2].

In most cases, PARP1 activity is induced through DNA-binding, resulting in PARylation of target proteins. PARP1 does, however, possess functions independent of its catalytic activity that are also dependent on interaction with DNA. PARP1 has long been related to the chromatin architectural protein H1. An inverse relationship between catalytically active PARP1 and H1 occurs at certain

transcriptionally active and repressed gene promoters [32]. At such promoters catalytically active PARP1 targets surrounding histones for PARylation, promoting chromatin relaxation. Interestingly, catalytically inactive PARP1 has also been shown to function in nucleosome compaction [30, 31, 33, 44]. PARP1 was found to localize to the *Drosophila* hsp70 promoter. When the hsp70 promoter was not expressed, PARP1 was localized to surrounding euchromatin in an inactive state. Upon induction, 'puffing' of the gene promoter was observed as a response to a robust increase in PAR at the promoter, indicating chromatin relaxation upon PARP1 activation [33]. Furthermore, atomic force microscopy (AFM) studies by the Kraus group demonstrated compaction of nucleosome arrays in the absence of NAD^+, the PARP1 substrate. Compaction of arrays was shown to be dependent on the presence of PARP1 constructs containing both the DNA-binding region and catalytic domain [30].

PARP1 is involved in many processes that are essential to cellular viability. Its roles in DNA-damage repair and genome stability have been widely researched, yet a steadfast mechanism has yet to be devised. The mode of regulation is a major missing piece to the PARP1 puzzle. Affinities generated using a developed FRET binding assay display a preference by PARP1 in binding to DNA models that have increased accessibility to core nucleotides. We also observe in binding affinity and stoichiometry experiments that PARP1 strength of interaction with mononucleosomes is dependent on linker-arm DNA length. Additionally, we observe that full-length PARP1 binds much tighter to both DNA substrates than a

truncated $Parp_{1-486}$ protein. Interestingly, the increased affinity in which full-length PARP1 binds as compared to $Parp_{1-486}$ is variable between binding to DNA constructs and mononucleosomes. These results indicate a possible means in which PARP1 regulates its function through variable binding affinities to DNA and nucleosome substrates.

Development of a high-throughput binding assay

Full-length PARP1 is highly toxic when expressed in bacterial cell lines. Due to this, a version of PARP1 that only contains the N-terminal half (Zn1, Zn2, Zn3 and BRCT auto-modification domain: residues 1-486) of PARP1 was produced. The $Parp_{1-486}$ construct is robustly expressed in *E. coli* after plasmid transformation, and purified through a straightforward method using Ni resin, ion-exchange, and size-exclusion chromatography. Previous experiments in our lab showed that $Parp_{1-486}$'s affinity for 30 bp blunt-ended, nicked, and 3'-overhang DNA's was in the range of 70-300 nM [8]. The characterization of $Parp_{1-486}$ dissociation constants (Kd's) to these DNA constructs was determined using fluorescent quenching of labeled DNA's using a Perkin-Elmer Victor 3V plate reader. Efficiency of the fluorescent quenching technique was limited due to the capabilities of the plate reader instrument, as well as complications with non-specific interactions by $Parp_{1-486}$ to the surface of the reaction vessel.

Much of my research has been devoted to the development of a high-throughput assay capable of measuring the thermodynamics of PARP1-DNA interactions in an efficient manner that is devoid of the non-specific PARP1 binding variable. After much trial and error I settled on an in-solution FRET-based assay utilizing Alexa 488 tagged $Parp_{1\text{-}486}$ donor and Cy5 labeled DNA acceptor (Atto 647 was substituted for Cy5 in nucleosomes). Non-specific interactions of PARP1 with reaction wells are not a problem in this system, as FRET-based measurements require limiting donor concentrations (5-fold to 10-fold below the measured Kd). As such, any amount of protein lost to non-specific interactions will not bias the FRET signal as long as the [donor] is 5-fold to 10-fold below the measured Kd.

The fluorescent labeling of $Parp_{1\text{-}486}$ is possible due to a fortunate structural characteristic of the truncated protein. $Parp_{1\text{-}486}$ contains 11 cysteine residues, 10 of which are incorporated in the three Zn containing motifs (Figure 4). Thus, only one cysteine residue (Cys 256) is left accessible to potential Alexa 488 binding. Successful preparation of Alexa 488-tagged $Parp_{1\text{-}486}$ was accomplished through mixing of protein and fluorophore overnight, followed by removal of free fluorophore through purification by a Hightrap-heparin HP cation-exchange column. Modification of N-terminally truncated PARP1 (487-1014) is also possible through fluorescent labeling of a cysteine residue in the catalytic domain. Thus, the full-length protein when exposed to Alexa488 fluorophore

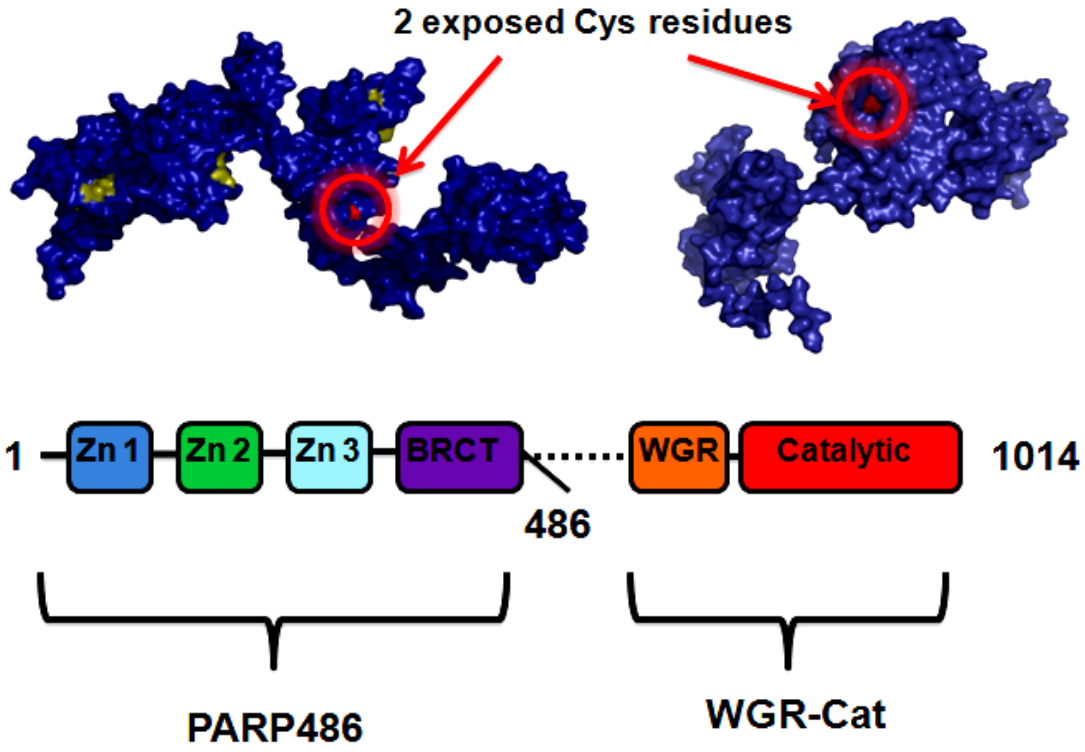

Figure 4- PARP1 contains two potential residues accessible to fluorophore modification. Molecular dynamics models as generated by Nicholas Clark of full-length PARP1 derived from small angle x-ray scattering (SAXS) with the exposed non-zinc coordinating residues shown in red. Images are representations of the $PARP_{1-486}$ construct and WGR-Cat region, each independent of the other. The $PARP_{1-486}$ construct contains 11 cys residues, 10 of which are encompassed in the three Zn containing motifs, while the WGR-Cat region contains only a single surface exposed cys residue. A single non-zinc coordinating cys residue in the DNA binding domain (cys 256) and surface exposed cys residue of the WGR-Cat (cys 845) region act as possible targets for fluorescent labeling.

becomes labeled at two different sites (Figure 4). Analysis by mass spectrometry confirmed respective single and double modifications of the two proteins (data not shown).

Each binding curve was obtained by a titration of fluorescently labeled binding substrate and a constant concentration of fluorescently labeled PARP1 (Figure 5). For signal correction purposes, each assay included labeled PARP1 (donor)-only wells (in quadruplicate) and a titration (paralleling the FRET titration) of labeled substrate (acceptor) only. Enhancement or quenching of the donor fluorophore was also controlled for with a titration series containing labeled donor and unlabeled substrate. No significant contribution to the overall FRET signal due to an increase in exposure or quenching of the donor molecule was observed in assays carried out with any PARP1 substrate. An additional correction was performed on images obtained using the donor emission wavelength band filter. Donor emission correction consisted of subtraction for acceptor fluorophore signal in the 'acceptor-only' wells from the FRET titration. This contribution can be significant due to the low [donor] and is necessary for the accurate calculation of dissociation constants. Final plotted values were corrected for acceptor signal contribution (calculated from 'acceptor-only' titration) and donor signal contribution (from 'donor-only' wells) according to the following equation:

$$FRETc = FRET - [(Dc \times FRET) + (Ac \times FRET)]$$

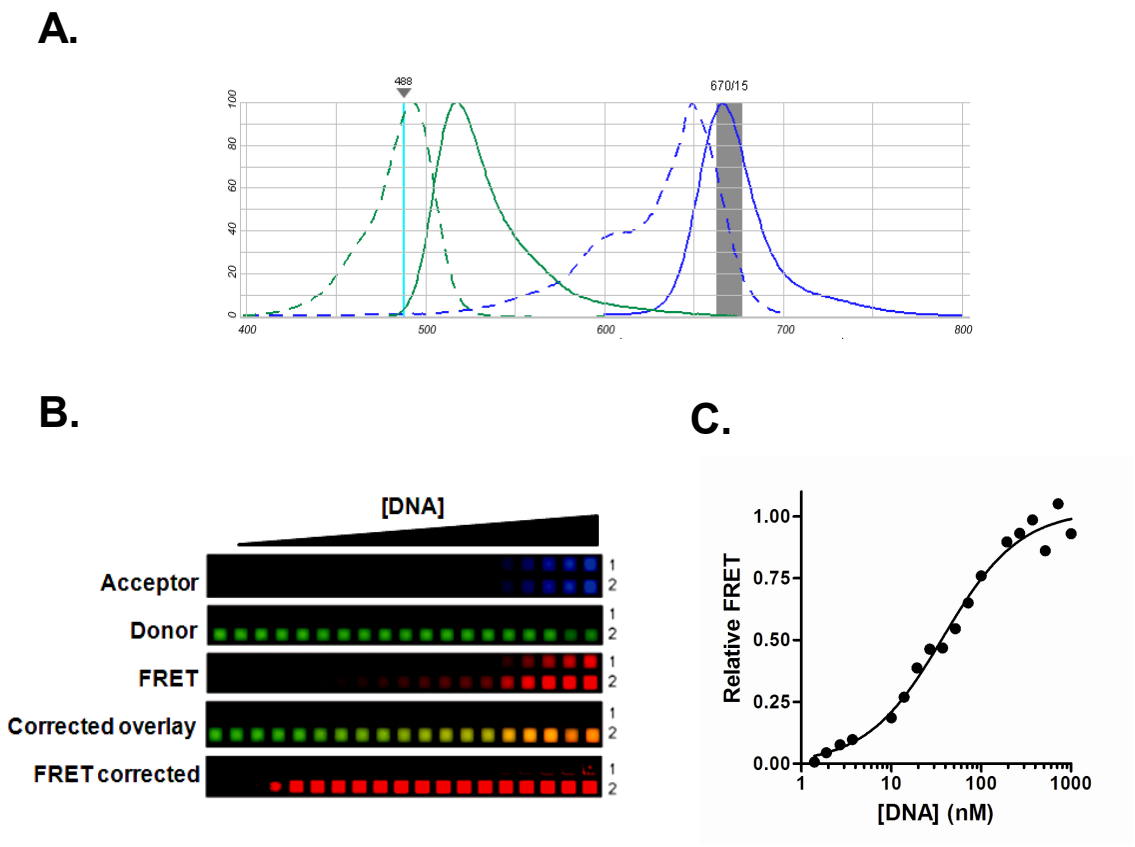

Figure 5- Interaction between PARP1 and DNA generates a FRET signal through energy transfer from donor to acceptor fluorophores. (A) Excitation **(dashed line)** and emission **(solid line)** of the Alexa488 fluorophore **(in green)** and Cy5 fluorophore **(in blue)**. Grey bar is representative of the emission band filter applied in FRET experiments using the Typhoon imager. Graph adapted from Invitrogen website **(B)** Fluorescent image of PARP1-DNA FRET assay produced by Typhoon scanner. Rows each image represent an acceptor-only control (1) and the FRET reaction with titrated acceptor and fixed [donor] (2). Each reaction is imaged using three different excitation laser and emission band filter combinations optimized to obtain isolated signals from acceptor DNA **(blue)**, protein donor **(green)**, and FRET reaction **(red)**. Corrected FRET overlay allows for visualization of increased production of energy transfer as DNA is titrated into a fixed [protein]. The final FRET signal utilized for generation of binding curves is normalized for donor and acceptor signal contribution. **(C)** Binding curve generated using prism software and corrected FRET data from images produced by Typhoon scanner, such as that observed in **(B)**, of $PARP_{1\text{-}486}$ binding affinity to 30bp blunt-end DNA construct.

where FRETc is final corrected FRET signal, FRET is total signal obtained using FRET excitation and emission settings, and Dc and Ac are percent contribution to overall FRET signal due to donor (D) and acceptor (A).

Mode of PARP1 DNA interaction

In addition to the $Parp_{1-486}$ *E. coli* expression system, other members in the Luger lab generated a system utilizing insect cell expression and purification of full-length PARP1. Both expression systems yield an efficient quantity of pure protein. The full-length PARP1 product, however, is much more susceptible to degradation and loss due to non-specific interactions with dialysis tubing and concentrators. The $Parp_{1-486}$ product is very stable and exhibits a lesser degree of non-specific interactions. It was hypothesized that truncated $Parp_{1-486}$ protein would suffice for DNA-binding studies, as the domains incorporated comprise the DNA-binding domain of PARP1. The DNA-binding domain of PARP1 has been found to be necessary and sufficient in PARP1 DNA-damage recognition and binding. As such, $Parp_{1-486}$ expressed from *E. coli* was used predominantly in PARP1-DNA interaction characterization.

In order to confirm the hypothesis that the $Parp_{1-486}$ mutant would suffice for binding studies, a comparison between $Parp_{1-486}$ and full-length PARP1's affinity to blunt-ended DNA was performed. Full-length PARP1 and $Parp_{1-486}$ affinity to blunt-ended DNA was measured at 200 mM NaCl. $Parp_{1-486}$ displayed an affinity

of ~ 45 nM, whereas full-length PARP1 bound approximately two-fold tighter with an affinity of ~ 26 nM (Figure 6). Previous studies have shown PARP1 loses specificity for DNA upon the loss of the Zn1 domain, and ΔZn2 constructs display greatly reduced affinity to DNA [9]. This indicates that the WGR-Cat region of PARP1 (487-1014) most likely only contributes in a stabilizing manner and is complementary to the $Parp_{1-486}$-DNA interaction. This would account for the approximate two-fold increase in binding affinity and indicate that the $Parp_{1-486}$ construct is sufficient in relative DNA-binding characterization studies.

While obtaining the $Parp_{1-486}$ affinity to blunt-ended DNA, an interesting discrepancy in $Parp_{1-486}$ affinity to the DNA substrate was observed. After further analysis it was noted that the only variable altered was the concentration of NaCl in the reaction buffer. Data previously published by our lab suggested a binding affinity of $Parp_{1-486}$ to blunt DNA of approximately 300 nM (fluorescent quenching experiments performed at 300 mM NaCl) [8]. In order to further explore an electrostatic dependence on binding, FRET-based binding assays were performed utilizing reaction buffer containing an [NaCl] gradient ranging from 175 mM NaCl to 250 mM NaCl (Figure 7B). A log(Kd) vs log[NaCl] plot yielded a linear electrostatic dependence for the $Parp_{1-486}$ to blunt-ended DNA interaction (Figure 7A). A slope of ~ 6 was generated from the linear fit of the log(Kd) vs log[NaCl] plot, indicating the presence of 6 ion pairs at the $Parp_{1-486}$-DNA

A.

	FLPARP	PARP486
DNA substrate	Blunt DNA	Blunt DNA
Kd (nM)	26.1 ± 4.5	44.7 ± 7.5
R^2	0.96	0.96

B.

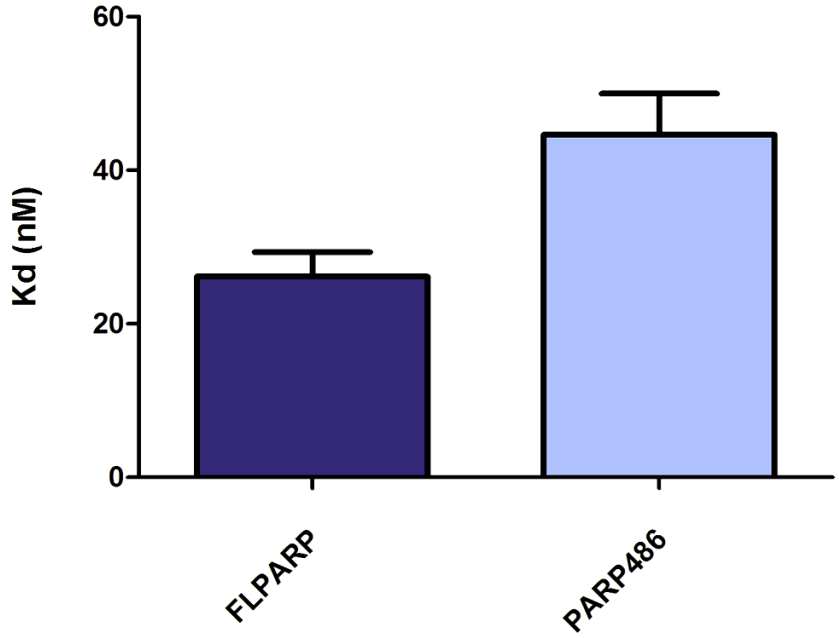

Figure 6- Full-length PARP1 binds with higher affinity to DNA damage models than the truncated $PARP_{1\text{-}486}$ construct. (A) Table displaying full-length PARP1 and $PARP_{1\text{-}486}$ affinities to blunt-ended DNA. Dissociation constants generated are the product of FRET assays performed with at least two biological replicates. Error bars are representative of one standard deviation. **(B)** Bar graph representative of observed affinities presented in the above table. Full-length PARP1 **(dark blue)** binds approximately 2-fold tighter to blunt-ended DNA than $PARP_{1\text{-}486}$ **(light blue)**.

A.

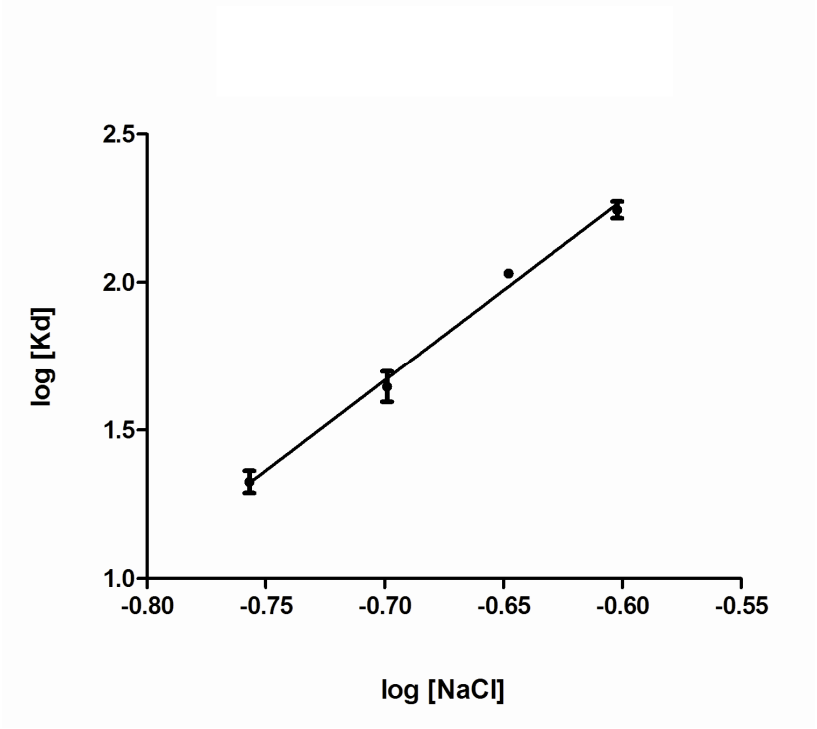

B.

[NaCl]	Kd (nM)	R^2
175 mM	21.23 ± 2.6	0.96
200 mM	44.66 ± 7.5	0.96
225 mM	107.25 ± 3.6	0.95
250 mM	189.2 ± 25	0.98

Figure 7- PARP1 interaction with DNA is dependent on [NaCl]. (A) Log(Kd) vs Log[NaCl] plot of $PARP_{1\text{-}486}$ affinity to blunt-ended DNA at 4 different [NaCl]. $PARP_{1\text{-}486}$ affinities were generated using the FRET-based assay after analysis of data produced by the Typhoon imager. Data points displayed are representative of at least two biological replicates and error bars were produced by a single standard deviation. A linear fit produces a slope of ~ 6, indicating the presence of 6 ion pairs at the $PARP_{1\text{-}486}$-DNA interface. **(B)** Table showing each [NaCl] tested with the corresponding $PARP_{1\text{-}486}$ affinities to blunt ended DNA.

interface. Similar electrostatic dependence was also observed when assaying additional DNA constructs (data not shown), indicating that the dependence is not unique to the blunt-ended DNA.

PARP1 preference for specific DNA architecture

To date, the PARP1-DNA interaction has not been shown to exhibit any DNA sequence specificity [1, 2]. It has been long known that PARP1 binds *in vitro* and *in vivo* to sites of DNA-damage, as well as to various unique DNA conformations void of DNA-damage, such as hairpin loops and cruciform DNA [1, 2]. In the literature, reliable data outlining the binding affinity of PARP1 to its proposed DNA partners is limited. Previous studies in our lab demonstrated that $Parp_{1\text{-}486}$ displays similar affinity to overhang and nicked DNA, which is approximately three times tighter than to blunt DNA (reaction performed with 300 mM NaCl) [8].

The developed in-solution FRET-based assay was first utilized to confirm previous data on $Parp_{1\text{-}486}$ affinity to blunt, nicked and overhang DNA. The blunt-ended and nicked DNA's were not altered from previous studies in the Luger lab [8]. A slight alteration to the overhang DNA was performed to better ensure the model was representative of a true overhang region. Rather than truncating one of the strands of the DNA double-helix to produce a single overhang, strands of 30 bps each were annealed in a fashion that yields two overhangs per DNA molecule (Figure 8A). $Parp_{1\text{-}486}$ was determined to bind with similar affinity to the

A.

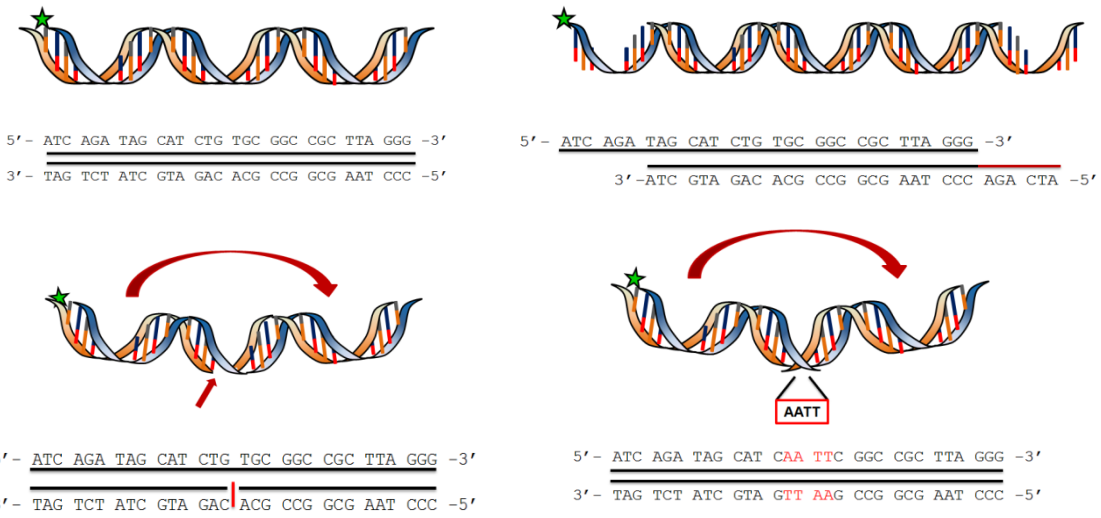

B.

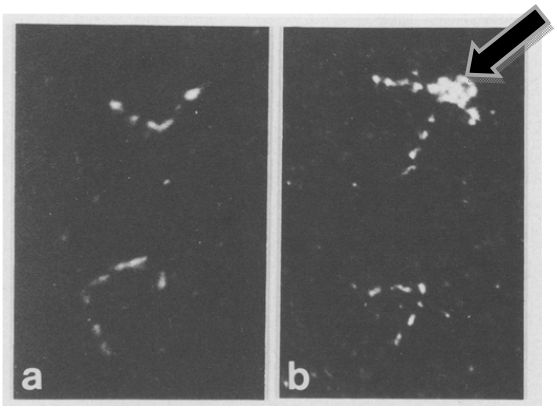

Figure 8- PARP1 binds various DNA substrates. (A) Graphic representations of DNA constructs used in FRET binding assays. From left to right, models are of blunt-ended DNA, 5'-overhang DNA **(top row)**, DNA with an internal 'nick' and DNA containing a central AATT sequence substitution yielding increased strand flexibility **(bottom row)**. DNA sequences are indicated below each corresponding model. Conserved sequences are displayed in **black** and significant changes to DNA strands are indicated in **red**. **(B)** Dark field microscopy displaying intrinsic flexibility of 139bp DNA which contains a central nick at base pair 69 in the absence of PARP1 **(left)** and with PARP1 bound **(arrow in right panel)** as adapted from de Murcia *et al.,* Mol Cell Biochem, 1994. 138(1-2): p. 15-24.

blunt-ended DNA and the overhang DNA (~45 nM), while exhibiting a binding affinity that was 3-5 times tighter to the nicked DNA (~10 nM) (Figure 9). In our lab's previous publication describing PARP1 affinities, the blunt-ended DNA was found to be a weaker binding substrate than both the 3'-overhang DNA and the nicked DNA, which PARP1 bound with similar affinity [8]. The results from the FRET-based assay differ from the previous publication in indicating that PARP1 binds blunt-ended DNA and 3'-overhang DNA with relatively the same affinity while binding nicked DNA ~ five-fold tighter. A similar affinity displayed by PARP1 for 3'-overhang DNA and blunt-ended DNA, which contrasts to its affinity to nicked DNA, is logical. This is due to the closer resemblance of 3'-overhang DNA and blunt-ended DNA to DSBs repaired through HR and NHEJ, compared to nicked DNA's relation to SSBs repaired via the BER pathway. It is possible non-specific interactions with reaction vessel surfaces had a more pronounced effect on past experiments than previously thought. Any variation in [$Parp_{1\text{-}486}$] due to non-specific interactions would lead to a shift in the affinity curve, as previous experiments used $Parp_{1\text{-}486}$ as the titrant, which is opposite of the FRET-based method utilized here. Additionally, the alteration in the 3'-overhang construct may have contributed to PARP1's affinity to the substrate.

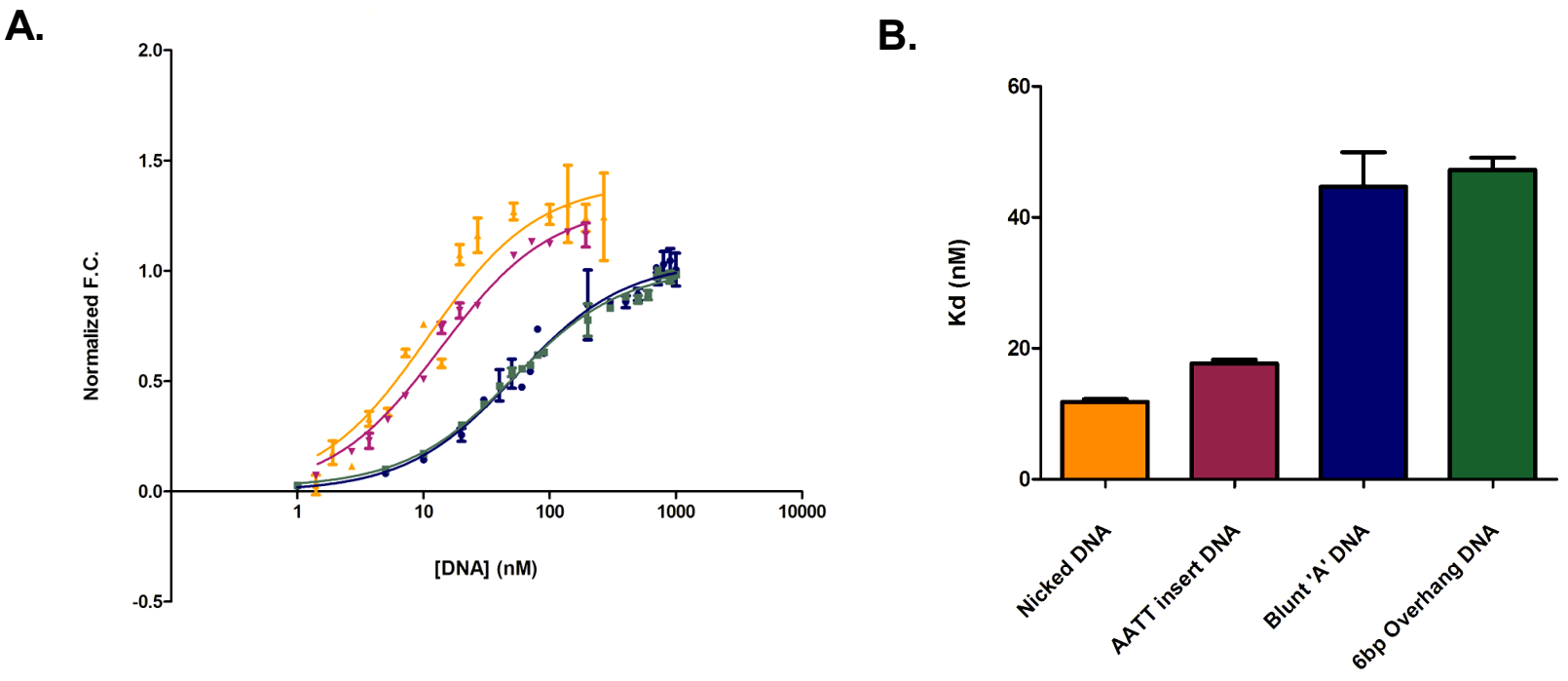

Figure 9 - Thermodynamic representation of $Parp_{1-486}$ interaction with various DNA-damage constructs. (A) Overlay of $Parp_{1-486}$-DNA-damage binding curves generated from FRET data obtained by the Typhoon imager. $Parp_{1-486}$ binds with highest affinity to 30mer DNA sequences containing a single, centrally located nick **(gold)** and DNA with induced flexibility due to an AATT-sequence insert **(purple)**. $Parp_{1-486}$ binds more weakly to DNA modeled after DSBs containing blunt ends **(blue)** and 3'-overhangs **(green)**. Each data point is representative of assays performed in biological replicate and error bars were generated using single standard deviation **(B)** Bar graph comparing observed Kd's for nicked DNA (~11nM), DNA containing an AATT insert (~17nM), blunt ended DNA (~45nM) and 3'-overhang DNA (~47nM). Increased flexibility upon AATT insertion into the center of the blunt DNA produces a three to five-fold increase in $Parp_{1-486}$ affinity to the DNA substrate.

DNA constructs composed of various sequences were generated to assess the effect of sequence alteration in PARP1's affinity to blunt-ended DNA. Unexpectedly, it was observed that $Parp_{1\text{-}486}$ bound to a 30mer sequence containing a stretch of A-T base pairs with an affinity considerably tighter than what was observed with the previously used 30mer blunt sequence (Figure 9B).

No previous data has been presented indicating sequence specificity in PARP1-DNA interactions. Due to this we evaluated other factors that may have contributed to the increase in affinity observed. Tracts of 4 or more A:T base pairs have been shown to induce flexibility in DNA sequences [56] (Figure 8B). For example, poly(A:T) tracts are incorporated into the 601 nucleosome-positioning sequence [57] due to past evidence displaying that nucleosomes tend to form on sequences with an increased degree of flexibility [53]. Past literature has also proposed a similar propensity for flexible DNA by PARP1 [58-60]. We explored the affinity of $Parp_{1\text{-}486}$ for DNA exhibiting a higher degree of flexibility through the incorporation of the same AATT sequence into the center of the previously tested 30mer blunt-ended DNA. $Parp_{1\text{-}486}$ affinity to blunt-ended DNA with an imbedded AATT sequence was similar to that of the nicked DNA (~15nM), indicating $Parp_{1\text{-}486}$ binds preferably to DNAs with increased flexibility (Figure 9). A proportional increase in affinity to blunt-ended DNA containing an AATT insert with full-length PARP1 was also observed (data not shown), indicating that the WGR-Cat region does not contribute to the discrepancy in binding affinity between the two DNA models.

PARP1-Nucleosome interaction

PARP1 and H1 have been shown to compete for nucleosome binding at promoter regions of transcriptionally active or repressed genes [32]. This indicates close proximity of PARP1 and H1 binding sites along chromatin. The Kraus group demonstrated that portions of the DNA-binding region and catalytic domain of PARP1 are necessary and sufficient for nucleosome array compaction [30]. These results suggest a characteristic difference between PARP1's mode of binding to DNA-damage models (in which the DNA-binding region is sufficient for proper interaction) and nucleosome complexes. To ensure binding affinity data generated on PARP1-nucleosome interactions was representative of the true biological mechanism, fluorescently labeled full-length PARP1 was utilized.

To investigate the PARP1 mode of interaction with nucleosomes, mononucleosomes containing varying DNA linker lengths were prepared. Mononucleosomes were assembled using DNA sequences with the 601 nucleosome positioning sequence [57], with lengths of 147bp, 165bp and 207bp (Figure 10A). 147bp of DNA make contact with the histone octamer forming the nucleosome core particle (NCP) [26]. Additional DNA lengths utilized in mononucleosome formation will generate nucleosomes with DNA linker arms of various length (0bp, 9bp, and 15bp; actual linker arm lengths vary due to slight

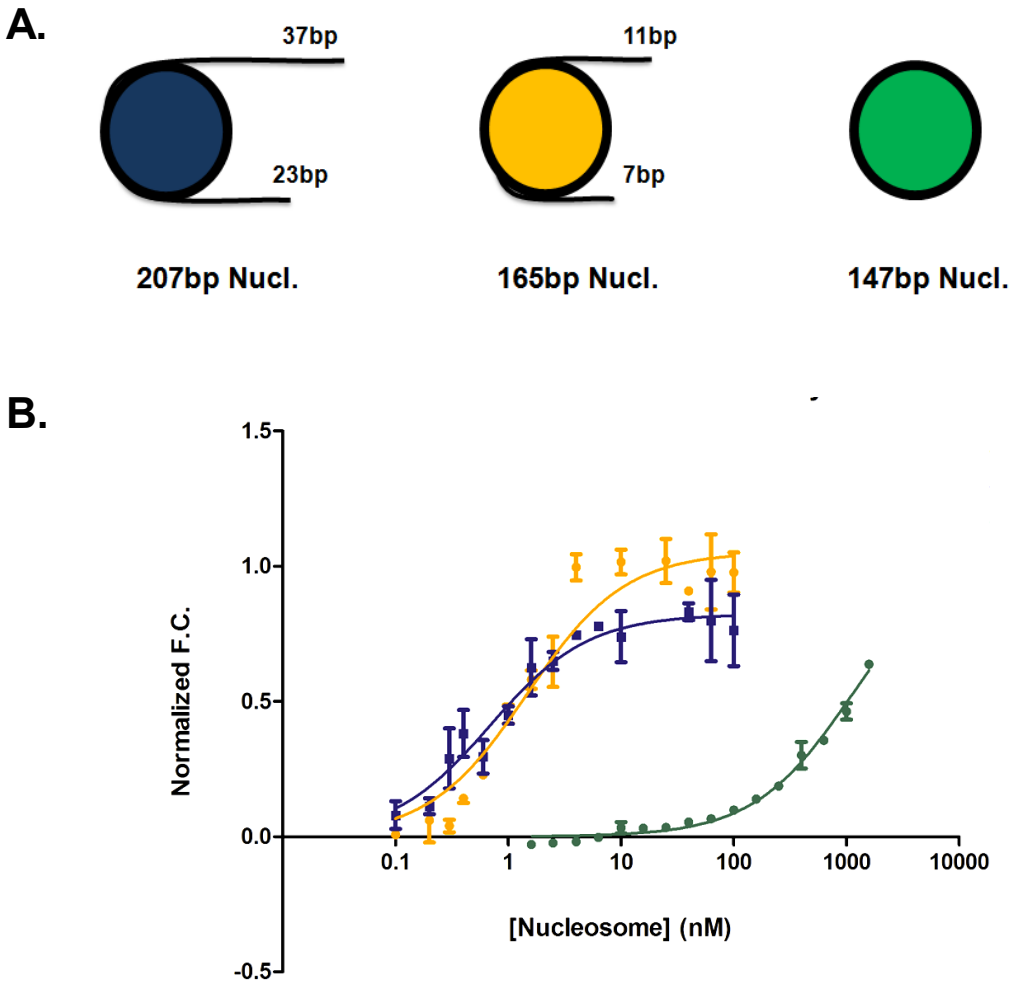

Figure 10- Full-length PARP1 binds tightly to nucleosomes containing linker DNA. (A) Models of mononucleosomes engineered with DNA mimicking regions of the 601 nucleosome-positioning sequence [51]. Mononucleosomes generated using 207bp **(blue)** and 165bp **(gold)** of DNA yield linker arms of ~ 30bp and ~10bp, respectively. Mononucleosomes produced using 147bp of DNA **(green)** do not have a sufficient length of DNA to produce linker arms. **(B)** Full-length PARP1 binds with an affinity of ~1nM to 165bp mononucleosomes **(gold)** and 207bp mononucleosomes **(blue)**. In comparison, full-length PARP1 binds very weakly to 147bp mononucleosomes **(green)**, which do not contain enough DNA to establish linker arms beyond the NCP. Dissociation constants were generated through measurement of increasing FRET throughout a titration of PARP1 substrate into constant [full-length PARP1]. Data points are representative of two biological replicates and error bars represent one standard deviation.

asymmetrical placement preference of the histone octamer (Figure 10A)). The integrity of mononucleosomes and absence of significant amounts of free DNA was confirmed by native gel electrophoresis.

Stoichiometry of the PARP1-mononucleosome complexes was measured by Nick Clark and Dr. Uma Muthurajan of the Luger lab. Full-length PARP1 and $Parp_{1\text{-}486}$ were able to bind and shift the 147, 165, and 207 bp mononucleosomes in EMSA experiments with a 1:1 binding ratio. The interaction observed in EMSA between PARP1 and the 147bp mononucleosomes was counter to our initial hypothesis that PARP1 interacts primarily with the linker DNA of mononucleosomes. To confirm the validity of the EMSA results, analytic ultracentrifugation (AUC) was performed on full-length PARP1 and mononucleosomes independent of each other and in complex. AUC clearly demonstrates an interaction of 1:1 stoichiometric ratio between full-length PARP1 and 165bp mononucleosomes, as well as with 207bp mononucleosomes. The full-length PARP1-147bp mononucleosome complex, however, was not stable in AUC. The PARP1-147bp mononucleosome complex observed in EMSA is possibly due to forced interaction as a result of spacial restriction by the gel pores. AUC stoichiometry results were verified using size-exclusion chromatography coupled with multiangle light scattering (SEC-MALS). All stoichiometry experiments were repeated with $Parp_{1\text{-}486}$ and yielded identical results, indicating that the DNA-binding region of PARP1 is able to bind mononucleosomes independently of the WGR and catalytic domain.

In an attempt to ascertain characteristic differences in binding between $Parp_{1\text{-}486}$ and full-length PARP1, which would assist in a rationalization of the chromatin compaction data procured by the Kraus group, affinities of $Parp_{1\text{-}486}$ and full-length PARP1 to the mononucleosome models were obtained. Reactions performed in the microplate FRET-based assay at 200 mM NaCl produced an approximate affinity of 1nM for the full-length PARP1 interaction with both 165bp and 207bp mononucleosomes (Figure 10B). Due to full-length PARP1's high affinity to the 165bp and 207bp mononucleosome complexes, only an approximate dissociation constant was obtained due to an inability to maintain the [donor] (full-length PARP1) 5-10-fold below the final Kd. Assays performed with varying donor concentrations (at least 2x below the predicted Kd) all produced affinities of approximately 1 nM, providing credence to the ascertained full-length PARP1 affinity to 165bp and 207bp mononucleosomes. FRET reactions containing full-length PARP1 and 147bp mononucleosomes did not produce a curve containing a plateau at high concentrations of acceptor, indicating a very low affinity for full-length PARP1 to 147bp mononucleosomes (Figure 10B).

$Parp_{1\text{-}486}$'s affinities to 147bp and 207bp mononucleosomes were then obtained via FRET microplate reactions. $Parp_{1\text{-}486}$ displayed an extremely weak affinity to 147bp mononucleosomes, with FRET measurements lacking an upper plateau in a manner similar to what was observed with full-length PARP1 (Figure 10). Additionally, compared to full-length PARP1, $Parp_{1\text{-}486}$ displayed a relatively weak

affinity to 207bp mononucleosomes (~95 nM) (Figure 11). $Parp_{1-486}$'s affinity to mononucleosomes containing linker arms is approximately 100-fold weaker than full-length PARP1 (Figure 11), as compared to a two-fold difference observed in binding affinities to DNA-damage models (Figure 6). The difference in relative binding affinities indicates different modes of interaction for full-length and $Parp_{1-486}$ with free DNA and nucleosomes, respectively.

A.

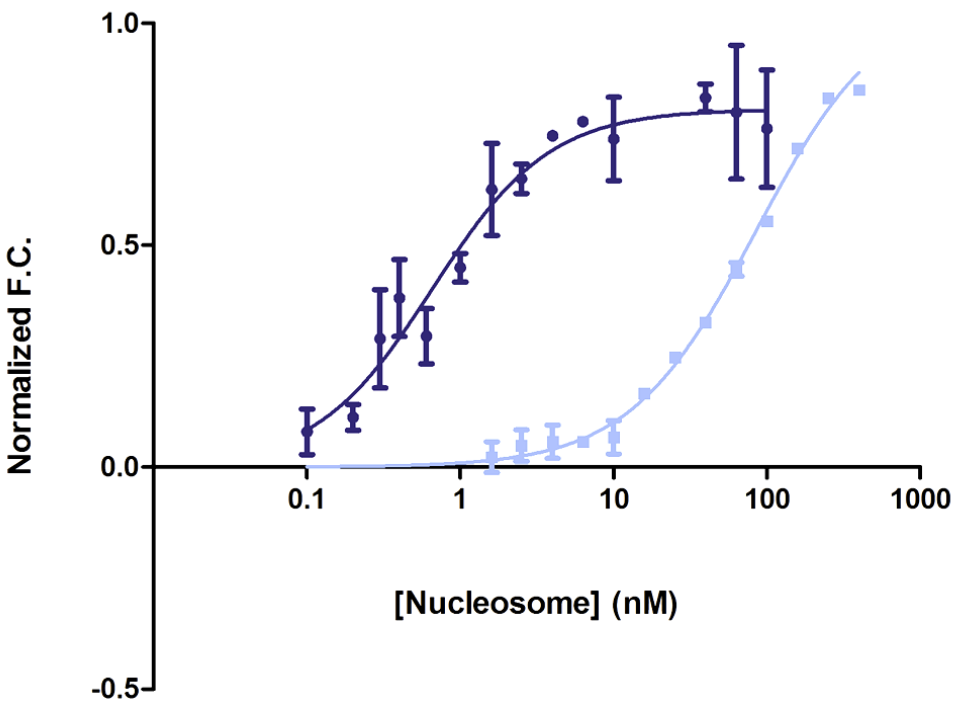

B.

	FLPARP	PARP486
Substrate	207 Nucl	207 Nucl
Kd (nM)	~ 1	94.5 ± 1.4
R^2	0.92	0.98

Figure 11- Full-length PARP11 binds with an affinity 100x tighter than Parp$_{1\text{-}486}$ to 207bp mononucleosomes. (A) Curves fit to data points obtained from FRET reactions imaged by the Typhoon scanner. Reactions were performed in biological replicate for reactions comprised of titrated substrate (0.1 nM-400 nM) and constant [PARP1] (0.5 nM in full-length PARP1 assays; 2 nM in PARP$_{1\text{-}486}$ assays). Error bars represent a single standard deviation. **(B)** Table of affinities generated from the above FRET data **(A)**. Due to limitations of the FRET system an exact dissociation constant for full-length PARP1 could not be obtained, but FRET assays carried out with various [probe] displayed Kd's within 0.6 nM to 1.5 nM. In comparison, PARP$_{1\text{-}486}$ binds much more weakly than full-length PARP1 to 207bp mononucleosomes, with an affinity of ~95nM.

DISCUSSION

Development of a high-throughput binding assay

The fluorescence quenching technique previously employed to obtain binding affinity data of the PARP1-DNA interaction was inefficient. This was due to issues with instrumentation and non-specific interactions between the protein and plate wells. I developed a FRET-based in-solution assay in place of fluorescent quenching. FRET utilizes the transfer of energy from the emission of a donor fluorophore to a nearby acceptor fluorophore. As such, FRET is a powerful tool when investigating proteins, such as PARP1, which displays a propensity to non-specifically interact with surfaces. In the assay developed here, non-specific interactions of PARP1 are negligible as a FRET signal is only produced upon protein-DNA interaction. Additionally, any emission from non-specifically interacting PARP1 can be corrected for in the overall FRET signal. It is important to note, however, that FRET is only effective if proper controls are employed to account for any unwanted contribution to the FRET signal.

The developed FRET-based assay exhibits high experimental efficiency due to the incorporation of microplates and the Typhoon imager. Microplates containing 384 wells allow for high efficiency, as up to four assays (23-point titration reactions in quadruplicate) can be performed on a single plate, all of which can be simultaneously quantified. Furthermore, consistency between assays is achieved through ensuring a consistent reaction environment in the microplate wells due to the employment of the hydrophobic coating (2% 1,6-dichlorooctamethyl-tetrasiloxane). Our FRET assay, coupled with the Typhoon imager, is highly sensitive. High sensitivity also allows for the use of low amounts of labeled donor (protein), making it possible to test a multitude of binding substrates without consuming large amounts of labeled protein. Because of these advantages, the FRET-based assay developed here is being incorporated within our lab to multiple other protein-binding systems, such as in the characterization of H1-nucleosome, MeCP2-nucleosome and Swc2-DNA interactions.

Mode of PARP1 DNA-binding

Recently, crystal structures of the first two Zn fingers of PARP1 in complex with blunt-end DNA was solved [9]. The crystal structure revealed that each Zn finger contains a hydrophobic loop that interacts via base stacking with exposed base pairs at the ends of the DNA, along with a ‘phosphate backbone grip’ loop that provides additional stabilization of the complex through contacts with the

phosphodiester backbone [9]. A log(Kd) vs log[NaCl] plot of $Parp_{1-486}$'s affinity to blunt-ended DNA indicates six ions pairs located at the $Parp_{1-486}$-DNA interface. This correlates well with the Zn finger-DNA crystal structures, where three positively charged residues are identified in the phosphate backbone grip of each Zn finger. Thus, our results concur with the Pascal group in identifying the phosphate backbone grip as providing electrostatic stabilization to the PARP1-DNA complex.

The domains excluded from the $Parp_{1-486}$ construct in the WGR-Cat region also contain a highly basic net charge. The two-fold increase in binding affinity exhibited by full-length PARP1 as compared to $Parp_{1-486}$ is most likely a result of the additional positive charge contained on the surface of the WGR-Cat region. Thus, an increase in [NaCl] could further diminish stabilization of PARP1 interaction with DNA substrates through neutralization of the additional positive charge located in the WGR-Cat region. The significant variabilition in DNA-binding affinity by PARP1 with NaCl concentration could be explained by the dependence on electrostatic stabilization of the PARP1-DNA complex by DNA backbone contacts made by PARP1's exposed basic residues.

PARP1 affinity is affected by specific DNA architecture

Binding data in the literature fails to establish a systematic approach to obtain PARP1's affinity to various DNA substrates. A commonly cited publication by D' Silva et al. derives dissociation constants for PARP1 from Lineweaver-Burk plots of PARP1 activity [61]. Added precaution must be exhibited in PARP1-DNA-binding studies due to PARP1's conformational change upon interaction with DNA. Using traditional enzyme kinetics to determine specific binding affinities in a multistep reaction, such as with PARP1 binding DNA, can be very difficult. As such, binding affinities obtained for PARP1 using this method are not as reliable as direct analysis of binding, such as in the FRET binding assay. As a result, they produce data suggesting PARP1 prefers DSB's over SSB's, which is contrary to what we observe using FRET.

Additionally, it is common practice to utilize surface plasmon resonance (SPR) when researching PARP1 binding properties. Although it is possible to characterize the PARP1-DNA complex utilizing SPR, a representation of native conditions in the cell are better achieved using the FRET-based assay. This is due to the FRET assay's employment of in-solution reactions. Furthermore, because a FRET signal is only produced upon PARP1-DNA interaction, any contribution from PARP1 binding to surfaces will not be detected, which is a possible variable to control for when using SPR.

Fluorescent quenching of DNA and fluorescence anisotropy have proven successful in characterization of the PARP1-DNA complex [8, 9]. Due to inefficiencies with methods and equipment, however, neither method provides a high-throughput system in which comparison of PARP1's affinity to different damage models can be performed.

The FRET binding assay I developed has the advantage of being unaffected by PARP1 non-specifically interacting with surfaces, because it directly analyzes PARP1 binding to DNA. Through utilization of our FRET-binding assay I was able to map PARP1 affinities to multiple DNA substrates. Of the DNA models we characterized, the blunt-ended DNA and overhang DNA best represent DSB's, whereas nicked DNA better mimics SSB sites found within the cell. Results of the FRET-based assay indicate that the DNA-binding domain of PARP1 prefers the nicked DNA, binding 3-5 times more tightly than blunt and overhang DNA.

Additionally, PARP1 displayed similar affinity to blunt-ended DNA containing a centrally located AATT sequence and nicked DNA. Dark-field microscopy and AFM data displays a visible bend in DNA strands containing a central incision in the phosphodiester backbone [60]. DNA sequences containing spans of four or more A-T base pairs have also been shown to have an induced bend and are

often used in nucleosome positioning sequences due to their flexible nature [56]. Thus, the similar affinity of PARP1 for nicked DNA and DNA containing an AATT insert appears to be due to the increased flexibility exhibited by both constructs.

Crystal structures of the first two Zn fingers of PARP1 independently in complex with blunt-ended DNA indicate that a single loop found in both Zn finger motifs contains two hydrophobic residues that interact with DNA base pairs exposed at the blunt ends through base stacking [9]. It is likely that PARP1's increase in affinity for DNA substrates displaying distortion in the form of a bend is due to an increase in accessibility of the Zn finger hydrophobic loops to DNA. Furthermore, due to the presence of nucleotides adjacent to both sides of PARP1's hydrophobic loop, additional base stacking may be achieved in the nicked and AATT insert models, possibly providing added stabilization to the interaction.

PARP1-Nucleosome interaction

PARP1 requires linker DNA for interaction with nucleosomes

PARP1 has been shown to play variable roles in gene expression via interactions with nucleosomes in a catalytically active and inactive manner [30, 31, 33].

The Kraus group showed that the DNA-binding region of PARP1 was necessary and sufficient for nucleosome binding, but that compaction of nucleosome arrays requires portions of the catalytic domain [30].

Here we further explore the PARP1-nucleosome complex through the observation of PARP1 binding affinity to mononucleosomes containing varied linker arm lengths. EMSA suggests that PARP1 has the ability to bind147bp, 165bp, and 207bp mononucleosomes through visualization of a band shift. AUC and SEC-MALS, however, indicate that full-length PARP1 and $Parp_{1\text{-}486}$ do not interact with 147bp mononucleosomes, while binding with a stoichiometry of 1:1 to 165bp and 207bp mononucleosomes. This demonstrates the unreliability of EMSA shifts in the indication of true interaction. Additionally, analysis of FRET-based studies indicates very weak binding of both full-length PARP1 and $Parp_{1\text{-}486}$ to 147bp mononucleosomes, implicating the necessity of linker DNA for PARP1-nucleosome interaction.

My results suggest that PARP1 binds with higher affinity to flexible DNA rather than blunt-ended DNA. Additionally, the PARP1 Zn fingers appear to interact with exposed base pairs through based stacking hydrophobic loops [9]. DNA wrapped around the histone octamer displays both of these characteristics. This poses the question, why doesn't PARP1 interact with DNA making contact with the histone octamer? To answer this question the orientation of PARP1 binding must be

understood. The PARP1 Zn fingers are connected by a flexible loop [1], providing them with multiple potential conformations in which they can interact with DNA. A binding mode in which the Zn fingers bound in series to DNA would likely permit PARP1 binding to DNA surrounding the histone octamer (Figure 12A). PARP1 binds to DNA with a footprint of 14 bps [53]. As such, if PARP1 bound in series to DNA surrounding the histone octamer, a potential binding ratio of ~ 10 PARP1 molecules per nucleosome would be observed. This is not the case, however, in our stoichiometry experiments, which display a 1:1 binding ratio. In addition, affinity experiments display very weak binding is observed by both full-length PARP1 and $Parp_{1\text{-}486}$ to mononucleosomes not containing DNA linker arms.

Alternatively, the Zn fingers may be interacting with DNA in a more offset, or 'clamped' conformation (Figure 12A). If the PARP1 Zn fingers bound with a clamped orientation to DNA any additional protein contacts made with the DNA substrate, such as with the histone octamer, would sterically inhibit PARP1 interaction. This models correlates with what was described with our results and is further supported by published crystallographic data [9].

A binding stoichiometry of 1:1 to mononucleosomes containing DNA linker arms is also interesting. PARP1 binds to blunt-ended DNA as short as 7bps [53] and as such, contains the ability to bind both DNA linker arms of mononucleosomes. Restriction of a second PARP1 molecule in the binding of 165bp and 207bp

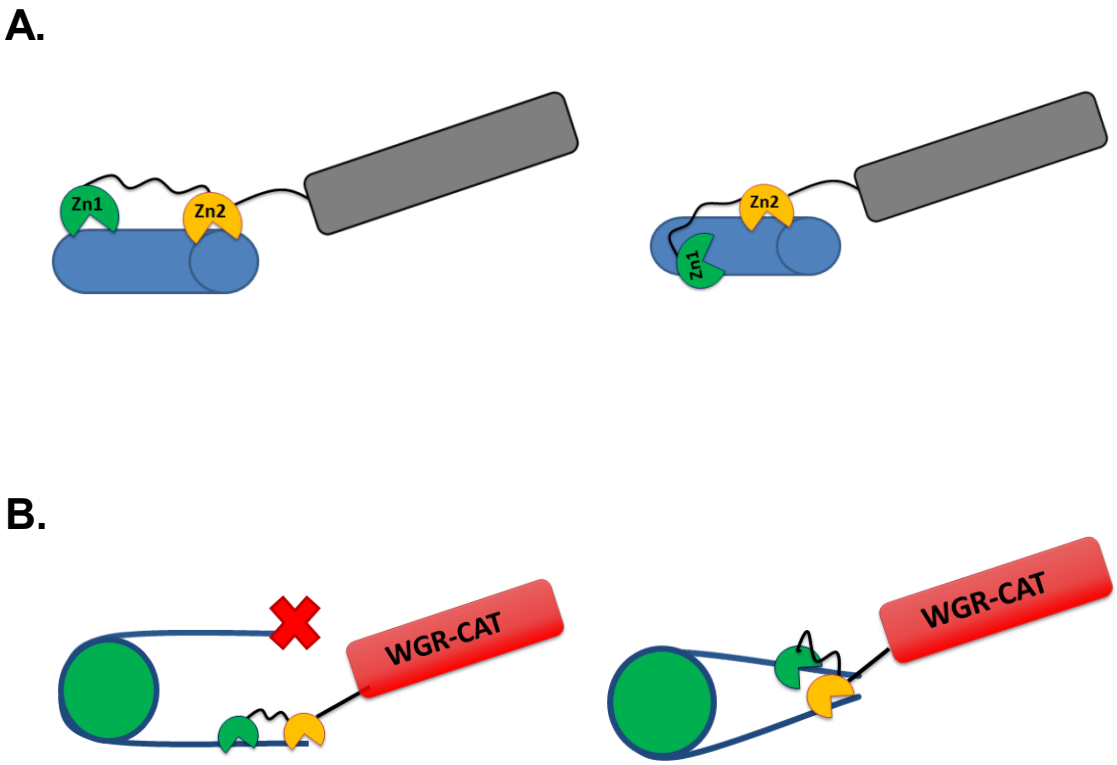

Figure 12- PARP1 binds to mononucleosomes containing DNA linker arms with a 1:1 stoichiometry. (A) PARP1 does not interact with DNA surrounding the histone octamer despite indications that it prefers DNA with exposed base pairs. Taking PARP1's binding preference and the flexible loop connecting the two Zn fingers **(green and gold)** into account two potential binding orientations are proposed. Zn1 and Zn2 may bind to DNA **(blue)** in series **(left)** or in a staggered 'clamp' orientation **(right)**. Our results imply the clamped conformation appears more likely as contacts made by the histones with DNA would better restrict the PARP1 Zn fingers from binding in this manner. **(B)** PARP1 binds to mononucleosomes with DNA linker arms **(blue)** in a 1:1 stoichiometry, indicating either blocking or occupation of the second linker arm. This may either occur by the WGR-Cat region of PARP1 blocking interaction by a second PARP1 molecule **(left)** or by occupancy of both DNA linker arms by PARP1 as it bridges the two blunt-ended strands **(right)**.

mononucleosomes suggests steric blocking or occupancy of the DNA linker arm. Blocking may occur due to the orientation of the initial PARP1 molecule bound to the other DNA linker arm (Figure 12B). Data has indicated that PARP1 binds with a specific orientation when bound to DNA [55]. The WGR-Cat region of PARP1 would likely inhibit binding of a second PARP1 molecule if orientated away from the NCP. A 1:1 stoichiometry is also observed, however, with $Parp_{1\text{-}486}$ which does not contain the large WGR-Cat region. It is possible that unbound Zn3 and BRCT domains contribute to steric hindrance of the second DNA linker arm, but this would likely be to a much lesser extent than the full-length protein. Restriction of the second DNA linker arm may also occur through bridging of the two linker arms by PARP1 (Figure 12B). Due to multiple DNA binding sites, PARP1 has the potential to interact with multiple DNA substrates in tandem. This may account for the 1:1 binding ratio observed in AUC and SEC-MALS and could provide insight into the mechanism by which PARP1 acts to condense chromatin.

Full-length PARP1 binds significantly more tightly to 207bp mononucleosomes than $Parp_{1\text{-}486}$

Full-length PARP1 binds tighter to 165bp and 207bp mononucleosomes than to the DNA-damage models representing DSBs or flexible DNA. The linker arms of the 165bp and 207bp mononucleosomes contain a high A-T content (~ 65% of entire linker sequence), with one linker arm containing a degree of flexibility due to a centrally located AATT stretch. The high A-T presence could itself be

responsible for the high affinity observed by full-length PARP1 to the engineered mononucleosomes. $Parp_{1\text{-}486}$, however, binds to 207 mononucleosomes with weak affinity as compared to DNA-damage models containing AT repeats. This indicates that dependence on DNA linker arm flexibility or AT content for PARP1 binding affinity is unlikely.

This prompts the question, what property of full-length PARP1 that is not present in $Parp_{1\text{-}486}$ gives it the capability to bind with such high affinity to mononucleosome linker arms? The two-fold discrepancy between full-length PARP1 and $Parp_{1\text{-}486}$ to DNA-damage constructs can be accounted for by the additional electrostatic stabilization contributed by the WGR-Cat region, which contains many exposed basic residues. An approximate 100-fold divergence between binding affinities, however, implies that while the DNA-binding region of PARP1 is necessary for nucleosome binding, it is not necessarily responsible for its strength of interaction.

Full-length PARP1 may exhibit two potential binding mechanisms which take into account binding affinity dependent on presence of the WGR-Cat region. (1) The WGR-Cat region may contribute additional stabilization of the interaction. This would be due to additional electrostatic contacts made due to an increased proximity to additional negatively charged DNA, or through specific contacts made by the WGR or catalytic domain with the nucleosome as is suggested in

the literature [30, 55]. Preliminary EMSA data shows, however, that truncation constructs containing only the WGR-Cat region do not interact with 147bp and 165bp mononucleosomes (data not shown). (2) It has been reported that PARP1 undergoes conformational change upon 30mer DNA-binding [9]. The presence of the WGR-Cat region at the C-terminus of PARP1 may allow for a more complete conformational change that cannot occur with $Parp_{1\text{-}486.}$ This conformational change would potentially lock the protein in a bound state, increasing the affinity of interaction. Additionally, induction of a locked conformation would limit the PARP1 dissociation rate.

This may act as a switch between PARP1's chromatin compaction and gene expression functions. After binding to chromatin, the PARP1-nucleosome interaction would remain stable until activation of PARP1. PARP1 would then promote chromatin relaxation while still bound to nucleosomes, allowing transcription to occur. Then, once a threshold of auto-modification by PARP1 occurs, a rapid release from chromatin would be promoted.

SUMMARY AND FUTURE DIRECTIONS

PARP1 and DNA-damage recognition

PARP1 maintains many functions within the cells through interactions with many different DNA substrates. Due to its prevalence in many cellular processes PARP1 has been targeted in drug therapies to treat medical conditions ranging from inflammation regulation to cancer. In order to better understand regulation of PARP1 function in the cell, it is necessary to analyze PARP1's interaction with DNA substrates. The most studied and possibly most significant mode of regulation exists in PARP1 recognition of DNA. It is possible this form of regulation occurs through discrepancies in binding affinity by PARP1 to DNA substrates during its various cellular functions. PARP1 interacts with DNA-damage models and nucleosomes, in what appears to be two different binding mechanisms.

I have developed a high-throughput *in vitro* binding assay to characterize PARP1's interaction with sites of DNA-damage and mononucleosomes. Our FRET-based assay has proved to be highly reproducible as well as acutely

sensitive. In addition, the FRET assay can be easily manipulated to incorporate the different interactions of PARP1, or any other fluorescently modifiable protein, forms with different cellular substrates.

Our results suggest a binding preference exhibited by PARP1 for DNA sequences permitting an increased accessibility to base pairs, such as DNA containing an internal nick or increased flexibility through the introduction of AT repeats. Binding affinity data presented here and structural data recently published on interactions by each Zn finger to blunt-ended DNA, convey a mechanism in which PARP1 recognizes sites of DNA-damage. PARP1 appears to primarily interact with DNA through hydrophobic loops present in the two Zn fingers. This interaction is stabilized through electrostatic interactions by highly basic regions located throughout the protein.

Additionally, results presented here suggest that $Parp_{1\text{-}486}$, which contains the DNA-binding domain of PARP1, binds slightly more weakly to DNA constructs mimicking DNA-damage than does full-length PARP1. This may be due to a significant electrostatic dependence on PARP1 binding affinity to DNA, as the full-length protein contains additional basic residues that could assist in PARP1-DNA complex stabilization.

These results have provided a quality start in the overall characterization of PARP1's interactions with non-nucleosomal DNA in the cell. Further studies carried out utilizing the FRET assay must be performed on PARP1's other known DNA partners to obtain a more complete understanding of its binding mechanism. Such substrates include DNA with non-canonical B-form architecture, hairpin loops and 4-way junction DNA (aka Holliday junction DNA). In addition, more insight into the role of PARP1 in transcription could be investigated. This would be accomplished through analysis of PARP1 affinity to promoter and insulator regions that it has been found to associate with while functioning in transcriptional regulation.

PARP1 and chromatin dynamics

PARP1 has also been identified as a major contributor to transcriptional regulation through modulation of chromosomal dynamics [1, 2, 32, 35, 38]. PARP1 functions to compact chromatin when catalytically inactive, and can promote chromatin relaxation through PARylation of core histones once activated. As a means to understand PARP1's variable function in chromatin dynamics we explored PARP1's affinity and stoichiometry to nucleosome structures.

It was observed that full-length PARP1 and $Parp_{1-486}$ require the presence of DNA linker arms in order to associate strongly with mononucleosomes. This was demonstrated by the lack of interaction of both constructs with mononucleosome constructs engineered with only 147 bps of DNA in AUC, SEC-MALS and the FRET binding assay. Full-length PARP1 and $Parp_{1-486}$ were found to bind with a 1:1 stoichiometry to 165bp and 207bp mononucleosomes. Additionally, full-length PARP1 was found to bind considerably more tightly to 207bp mononucleosomes than $Parp_{1-486}$, suggesting a PARP1 binding mechanism to mononucleosomes that does not parallel what is observed with its binding to sites of DNA-damage.

Two mechanisms were proposed in which the WGR-Cat region of PARP1 plays a significant role in establishing high affinity to mononucleosomes containing DNA linker arms. First, full-length PARP1 binding to nucleosomes may be stabilized through additional contacts made by the WGR or catalytic domain to the nucleosome. Such contacts may either be additional electrostatic stabilization or direct interaction with the histone octamer. Alternatively, the presence of the WGR-Cat region may be necessary to produce a more complete conformational change than what is seen with $Parp_{1-486}$ upon binding to nucleosomes. Preliminary result suggest the latter is more likely, as truncation constructs containing the WGR-Cat region do not shift 147bp or 165bp mononucleosomes.

In order to confirm this mechanism, more tests must be performed on the affinity of PARP1 to mononucleosomes. Sequentially decreasing the lengths of DNA linker arms would allow determination of the minimum amount of DNA needed for PARP1 to bind mononucleosomes. Additionally, mononucleosomes produced containing DNA linker arms without DNA ends could be employed to test PARP1s dependence on blunt ends for binding. This would be performed using either nucleosomes formed on plasmid DNA, or mononucleosomes containing biotinylated ends that could be joined together by streptavidin. Additionally, compaction of DNA linker arms can be assessed utilizing our FRET assay and the transfer of the donor FRET label to the linker DNA. Compaction would then be observed through monitoring FRET levels upon introduction of unlabeled PARP1.

A potential alteration in binding affinity by PARP1 to mononucleosomes with introduced sites of damage, such as nicks or lesions, could also be investigated. In order to test this, binding assays with full-length PARP1 and $Parp_{1\text{-}486}$ to 147bp mononucleosomes after introduction of damage regions would be performed. Sites of damage would be induced by hydroxyl radical exposure or induction through PCR of specific sites of damage into the 147bp DNA prior to mononucleosome assembly. In addition, PARP1 binding to wild-type nucleosome arrays and damage-incorporated nucleosome arrays could be analyzed by FRET

and AFM. These results would provide information regarding the events that unfold as PARP1 recognizes sites of DNA-damage after associating with nucleosomes.

Additional PARP1 research in development

Additional experiments presently in progress will also provide further insight into the PARP1 binding mechanism. Systems currently undergoing development focus on PARP1 activity upon substrate binding and structural characterization of the full-length PARP1-DNA complex through x-ray crystallography and small angle x-ray/neutron scattering. Activity analysis of PARP1 upon binding to different substrates is essential to complete characterization of PARP1's interactions within the cell. We have formulated a hypothesis in which PARP1 recognizes and binds to DNA substrates, producing a conformational change that generates variable activation corresponding to PARP1's affinity to the given substrate. Regulation of catalytic activity through a conformation change induced upon substrate binding would account for the PARP1's ability to distinguish between its many functions.

PARP1 is involved in cellular pathways ranging from mitotic spindle apparatus formation to cell-death signaling [1]. Due to its many roles in the cell, a clear indication of how PARP1 regulates its function has been difficult to obtain. Data presented here provide a foundation for a further research on the PARP1 binding

mechanism. Detailed comparison of PARP1 affinity to its various DNA-binding partners, along with additional PARP1 activation and structural data will produce a more unified understanding of how PARP1 maintains variable functions throughout the cell.

From a larger scope, a more unified understanding of PARP1 function in the cell is necessary as multiple cancer treatments target PARP1 as a method in chemotherapy. Such methods incorporate drugs acting to inhibit PARP1 function, as PARP1 inhibition leads to DNA-damage propagation. DNA-damage propagation in cells, including cancer cells, frequently leads to cell-death. Such drugs, however, fail to account for PARP1's many other roles in the cell. PARP1 inhibition has also been tied to the production of cancer cells, due to PARP1's intricate and diverse involvement in cellular function. As such, PARP1 inhibition as a cancer treatment has the potential to give rise to secondary malignancies, making such cancer therapies ultimately limited, even if effective. Further investigation of a variable PARP1 binding mechanism may provide additional targets in selective inhibition of PARP1. Selective inhibition would add power to cancer therapies targeting PARP1 and reduce the potential for secondary malignancies [3, 4].

REFERENCES

1. Ame, J.C., C. Spenlehauer, and G. de Murcia, *The PARP superfamily.* Bioessays, 2004. **26**(8): p. 882-93.
2. D'Amours, D., et al., *Poly(ADP-ribosyl)ation reactions in the regulation of nuclear functions.* Biochem J, 1999. **342 (Pt 2)**: p. 249-68.
3. McCabe, N., et al., *BRCA2-deficient CAPAN-1 cells are extremely sensitive to the inhibition of Poly (ADP-Ribose) polymerase: an issue of potency.* Cancer Biol Ther, 2005. **4**(9): p. 934-6.
4. Telli, M.L. and J.M. Ford, *PARP Inhibitors in Breast Cancer.* Clin Adv Hematol Oncol. **8**(9): p. 629-35.
5. Dantzer, F., et al., *Poly(ADP-ribose) polymerase-1 activation during DNA damage and repair.* Methods Enzymol, 2006. **409**: p. 493-510.
6. Langelier, M.F., et al., *A third zinc-binding domain of human poly(ADP-ribose) polymerase-1 coordinates DNA-dependent enzyme activation.* J Biol Chem, 2008. **283**(7): p. 4105-14.
7. Hitomi, K., S. Iwai, and J.A. Tainer, *The intricate structural chemistry of base excision repair machinery: implications for DNA damage recognition, removal, and repair.* DNA Repair (Amst), 2007. **6**(4): p. 410-28.
8. Lilyestrom, W., et al., *Structural and biophysical studies of human PARP-1 in complex with damaged DNA.* J Mol Biol, 2009. **395**(5): p. 983-94.
9. Langelier, M.F., et al., *Crystal structures of poly(ADP-ribose) polymerase-1 (PARP-1) zinc fingers bound to DNA: structural and functional insights into DNA-dependent PARP-1 activity.* J Biol Chem, 2011.
10. Huletsky, A., et al., *The effect of poly(ADP-ribosyl)ation on native and H1-depleted chromatin. A role of poly(ADP-ribosyl)ation on core nucleosome structure.* J Biol Chem, 1989. **264**(15): p. 8878-86.
11. Poirier, G.G., et al., *Poly(ADP-ribosyl)ation of polynucleosomes causes relaxation of chromatin structure.* Proc Natl Acad Sci U S A, 1982. **79**(11): p. 3423-7.
12. Mathis, G. and F.R. Althaus, *Release of core DNA from nucleosomal core particles following (ADP-ribose)n-modification in vitro.* Biochem Biophys Res Commun, 1987. **143**(3): p. 1049-54.
13. Bertram, C and Hass, R., *Cellular responses to reactive oxygen species-induced DNA damage and aging.* Biol Chem, 2008(1431-6730 (Print)).
14. Lindahl, T., *Instability and decay of the primary structure of DNA.* Nature, 1993. **362**(6422): p. 709-15.
15. Ciccia, A. and S.J. Elledge, *The DNA damage response: making it safe to play with knives.* Mol Cell, 2010(1097-4164 (Electronic)).

16. Simbulan-Rosenthal, C.M., et al., *Regulation of the expression or recruitment of components of the DNA synthesome by poly(ADP-ribose) polymerase.* Biochemistry, 1998. **37**(26): p. 9363-70.
17. Sukhanova, M., Khodyreva, S and Lavrik, O., *Poly(ADP-ribose) polymerase 1 regulates activity of DNA polymerase beta in long patch base excision repair.* Mutat Res, 2010(0027-5107 (Print)).
18. Strom, C.E., et al., *Poly (ADP-ribose) polymerase (PARP) is not involved in base excision repair but PARP inhibition traps a single-strand intermediate.* Nucleic Acids Res, 2010.
19. Rothkamm, K., et al., *Pathways of DNA double-strand break repair during the mammalian cell cycle.* Mol Cell Biol, 2003. **23**(16): p. 5706-15.
20. Hartlerode, A.J. and R. Scully, *Mechanisms of double-strand break repair in somatic mammalian cells.* Biochem J, 2009. **423**(2): p. 157-68.
21. Wang, M., et al., *PARP-1 and Ku compete for repair of DNA double strand breaks by distinct NHEJ pathways.* Nucleic Acids Res, 2006. **34**(21): p. 6170-82.
22. Mansour, W.Y., T. Rhein, and J. Dahm-Daphi, *The alternative end-joining pathway for repair of DNA double-strand breaks requires PARP1 but is not dependent upon microhomologies.* Nucleic Acids Res. **38**(18): p. 6065-77.
23. Saleh-Gohari, N. and T. Helleday, *Conservative homologous recombination preferentially repairs DNA double-strand breaks in the S phase of the cell cycle in human cells.* Nucleic Acids Res, 2004. **32**(12): p. 3683-8.
24. Claybon, A., et al., *PARP1 suppresses homologous recombination events in mice in vivo.* Nucleic Acids Res, 2010(1362-4962 (Electronic)).
25. Sugimura, K., et al., *PARP-1 ensures regulation of replication fork progression by homologous recombination on damaged DNA.* J Cell Biol, 2008. **183**(7): p. 1203-12.
26. Luger, K., et al., *Crystal structure of the nucleosome core particle at 2.8 A resolution.* Nature, 1997. **389**(6648): p. 251-60.
27. McGhee, J.D. and G. Felsenfeld, *Nucleosome structure.* Annu Rev Biochem, 1980. **49**: p. 1115-56.
28. Syed, S.H., et al., *Single-base resolution mapping of H1-nucleosome interactions and 3D organization of the nucleosome.* Proc Natl Acad Sci U S A. **107**(21): p. 9620-5.
29. Kimura, A., K. Matsubara, and M. Horikoshi, *A decade of histone acetylation: marking eukaryotic chromosomes with specific codes.* J Biochem, 2005. **138**(6): p. 647-62.
30. Wacker, D.A., et al., *The DNA Binding and Catalytic Domains of Poly(ADP-ribose) Polymerase-1 Cooperate in the Regulation of Chromatin Structure and Transcription.* Mol Cell Biol, 2007.
31. Kim, M.Y., et al., *NAD+-dependent modulation of chromatin structure and transcription by nucleosome binding properties of PARP-1.* Cell, 2004. **119**(6): p. 803-14.

32. Kraus, W.L., *Transcriptional control by PARP-1: chromatin modulation, enhancer-binding, coregulation, and insulation.* Curr Opin Cell Biol, 2008. **20**(3): p. 294-302.
33. Tulin, A. and A. Spradling, *Chromatin loosening by poly(ADP)-ribose polymerase (PARP) at Drosophila puff loci.* Science, 2003. **299**(5606): p. 560-2.
34. Frizzell, K.M., et al., *Global analysis of transcriptional regulation by poly(ADP-ribose) polymerase-1 and poly(ADP-ribose) glycohydrolase in MCF-7 human breast cancer cells.* J Biol Chem, 2009. **284**(49): p. 33926-38.
35. Krishnakumar, R. and W.L. Kraus, *PARP-1 regulates chromatin structure and transcription through a KDM5B-dependent pathway.* Mol Cell, 2010. **39**(5): p. 736-49.
36. Krishnakumar, R., et al., *Reciprocal binding of PARP-1 and histone H1 at promoters specifies transcriptional outcomes.* Science, 2008. **319**(5864): p. 819-21.
37. Quenet, D., et al., *The role of poly(ADP-ribosyl)ation in epigenetic events.* Int J Biochem Cell Biol, 2009. **41**(1): p. 60-5.
38. Cohen-Armon, M., et al., *DNA-independent PARP-1 activation by phosphorylated ERK2 increases Elk1 activity: a link to histone acetylation.* Mol Cell, 2007. **25**(2): p. 297-308.
39. van Wijk, S.J. and G.J. Hageman, *Poly(ADP-ribose) polymerase-1 mediated caspase-independent cell death after ischemia/reperfusion.* Free Radic Biol Med, 2005. **39**(1): p. 81-90.
40. Petermann, E., C. Keil, and S.L. Oei, *Importance of poly(ADP-ribose) polymerases in the regulation of DNA-dependent processes.* Cell Mol Life Sci, 2005. **62**(7-8): p. 731-8.
41. d'Adda di Fagagna, F., et al., *Functions of poly(ADP-ribose) polymerase in controlling telomere length and chromosomal stability.* Nat Genet, 1999(1061-4036 (Print)).
42. Salvati, E., et al., *PARP1 is activated at telomeres upon G4 stabilization: possible target for telomere-based therapy.* Oncogene. **29**(47): p. 6280-93.
43. Gomez, M., et al., *PARP1 Is a TRF2-associated poly(ADP-ribose)polymerase and protects eroded telomeres.* Mol Biol Cell, 2006. **17**(4): p. 1686-96.
44. Kim, M.Y., T. Zhang, and W.L. Kraus, *Poly(ADP-ribosyl)ation by PARP-1: 'PAR-laying' NAD+ into a nuclear signal.* Genes Dev, 2005. **19**(17): p. 1951-67.
45. Wessels, J.T., et al., *Advances in cellular, subcellular, and nanoscale imaging in vitro and in vivo.* Cytometry A, 2010. **77**(7): p. 667-76.
46. Stryer, L., *Fluorescence energy transfer as a spectroscopic ruler.* Annu Rev Biochem, 1978. **47**: p. 819-46.
47. Clegg, R.M., *The Vital Contributions of Perrin and Forster.* Biophotonics Intl. , 2004(11): p. 42-45.

48. Stryer, L. and R.P. Haugland, *Energy transfer: a spectroscopic ruler.* Proc Natl Acad Sci U S A, 1967. **58**(2): p. 719-26.
49. Latt, S.A., H.T. Cheung, and E.R. Blout, *Energy Transfer. A System with Relatively Fixed Donor-Acceptor Separation.* J Am Chem Soc, 1965. **87**: p. 995-1003.
50. Wu, P. and L. Brand, *Resonance energy transfer: methods and applications.* Anal Biochem, 1994. **218**(1): p. 1-13.
51. Thomas, J.O., *HMG1 and 2: architectural DNA-binding proteins.* Biochem Soc Trans, 2001. **29**(Pt 4): p. 395-401.
52. Starr, D.B., B.C. Hoopes, and D.K. Hawley, *DNA bending is an important component of site-specific recognition by the TATA binding protein.* J Mol Biol, 1995. **250**(4): p. 434-46.
53. Segal, E. and J. Widom, *What controls nucleosome positions?* Trends Genet, 2009. **25**(8): p. 335-43.
54. Harrison, S.C., *A structural taxonomy of DNA-binding domains.* Nature, 1991(0028-0836 (Print)).
55. Huambachano, O., et al., *The double-stranded DNA binding domain of poly(ADP-ribose) polymerase-1 and molecular insight into the regulation of its activity.* J Biol Chem.
56. Koo H.S., Wu, H.M. and Crothers, D.M., *DNA bending at adenine . thymine tracts.* Nature, 1986(0028-0836 (Print)).
57. Lowary, P.T. and J. Widom, *New DNA sequence rules for high affinity binding to histone octamer and sequence-directed nucleosome positioning.* J Mol Biol, 1998. **276**(1): p. 19-42.
58. Petrucco, S., *Sensing DNA damage by PARP-like fingers.* Nucleic Acids Res, 2003. **31**(23): p. 6689-99.
59. Sastry, S.S., K.G. Buki, and E. Kun, *Binding of adenosine diphosphoribosyltransferase to the termini and internal regions of linear DNAs.* Biochemistry, 1989. **28**(13): p. 5670-80.
60. de Murcia, G., et al., *Structure and function of poly(ADP-ribose) polymerase.* Mol Cell Biochem, 1994. **138**(1-2): p. 15-24.
61. D'Silva, I., et al., *Relative affinities of poly(ADP-ribose) polymerase and DNA-dependent protein kinase for DNA strand interruptions.* 1999(0006-3002 (Print)).